1-1-2012

# Fiber Bragg Grating Sensors For The Detection Of Metal Crack Initiation By Low Cycle Fatigue Test

KM M. Hossain
*Ryerson University*

# FIBER BRAGG GRATING SENSORS FOR THE DETECTION OF METAL CRACK INITIATION BY LOW CYCLE FATIGUE TEST

By

KM Mahmud Hossain

Bachelor of Science in Engineering (Telecommunication)

Khulna University of Engineering and Technology, Khulna, Bangladesh

June, 1999

A Thesis

Presented to Ryerson University as part of Master of Applied Science in the program of

Electrical and Computer Engineering

Toronto, Ontario, Canada, 2012

## AUTHOR'S DECLEARTION

I hereby declare that I am the sole author of this thesis.

I authorize Ryerson University to lend this thesis to any other institution or to any individual for the purpose of scholarly research.

_____

KM Mahmud Hossain

I further authorize Ryerson University to reproduce this thesis by photocopying or by other means, in total or in part, at the request of other institutions or individuals for the purpose of scholarly research.

_____

KM Mahmud Hossain

## Abstract

**FIBER BRAGG GRATING SENSORS FOR THE DETECTION OF METAL CRACK INITIATION BY LOW CYCLE FATIGUE TEST**

Master of Applied Science, 2012

KM Mahmud Hossain

Electrical and Computer engineering, Ryerson University

Structural integrity is always an important issue for the service life time of any structure. Therefore, joint of the metal is also a vital point to consider. This thesis describes a new method that uses the Fiber Bragg Grating (FBG) sensor to detect the crack initiation of friction stir welded aluminum (AL) alloy by low cycle fatigue test. Experimental setups and procedures are studied, a proper test configuration is determined and a series of testing performed. The applicability of this new method of stress control fatigue test in monitoring the metal crack initiation is demonstrated through the test results, which shows that FBG sensors are sensitive to capture the onset of the crack. Stress controlled fatigue tests especially at high strain amplitude for Friction Stir Welded (FSW) joints demand the sensors to withstand strain level above ±8000 με [40] and with the size of few mm, and these sensors are not available in the market. In this work, the new sensors arrays are used in the characterization of cyclic deformation behavior of FSW aluminum alloy, which, in some cases, could sustain up to ±11000με. During the experiment significant difference in plastic strain amplitude (PSA) was observed using these optical fiber sensors mounted in nugget zone (NZ) and across the boundary area between thermo mechanical affected zone (TMZ) and heat affected zone (HZ). For all the samples of Al alloy, with the progress of cyclic deformation the cyclic hardening characteristics of the metal were observed.

**ACKNOWLEDGEMENT'**S

I would like to convey my sincere gratitude and thanks to my supervisor, Dr. Xijia Gu, for his continued support and guidance. His enthusiasm and passion to the research work was a motivating factor for me throughout my study period at Ryerson University. I would also like to thank him for providing financial support to complete my graduate study.

I would like to thank Dr. Daolun Chen for his knowledge sharing and the enormous support he provided in designing and under taking the experiments.

I would like to thanks Mrs. Jiang Li, who provided me with all the guidance and assistance in preparing experiments. I would also thank to Wen Xu, who collaborated with me in my research and I gained better understanding fatigue test especially with the Instron Controller 8801 fatigue Testing System. I must mention and convey my gratitude to Mr. C. Li for extending his cooperation to share knowledge about data analysis and sample bonding.

Finally, I would like to express thanks to my family, specially my parents, my wife Sharmin Islam and to my children without their patient understanding and support, I could not finish my studies effectively.

**Table of Contents**

**List of Figures**

## Chapter 1

### 1. Introduction

The low density metals like aluminum and magnesium alloys are becoming more attractive than the conventional materials due to their high strength and also to high strength to weight ratios [1]. The technology of optical fibres has progressed very rapidly in recent years. Fiber Bragg Grating (FBG) is one of the key components in modern optical fiber communications and sensor systems. Many applications have been identified and demonstrated and the gratings are also available commercially. FBG has also become very popular because of its high dynamic range, immunity to electromagnetic interference and its multiplexing capability [2]. FBG's as short as 1 to 5 mm length, can be made on fibers of 125 μm in cladding diameter and was used in localized strain measurements recently [3]. However, FBG has a limitation of obtaining less strain reading than the true substrate strain with conventional bonding method due to the limited contact area between the fiber and substrate and due to shear modulus of the epoxy. Typically the FBG sensor is used when the strain variation is less than 3000με [1]. To overcome this problem, a new type of FBG sensor and a more robust bonding process are developed to measure high strain amplitude, to detect crack- initiation and to observe the metal behavior change with varying stress level.

In this thesis, it is demonstrated that the strain amplitude up to ± 11000 με can be reached by using flat-cladding FBG sensors applied to the fatigue test of aluminum alloy substrates. In tests, asymmetric hysteresis loops and non-uniform hardening and softening in the different zones of the alloy substrate was observed. The FBG sensors could also be applied to measure the localized strain variations to measure the distributed strain in materials and to monitor the structural health.

## 2. **Literature Survey**

Low-cycle fatigue tests subject specimens to repeated stress or strain until failure occurs at a relatively small number of cycles. The upper limit in lower cycle life has generally been selected arbitrarily by individual investigators to lie in the range of $10^4$ to $10^5$ cycles [4].

Investigations in low-cycle fatigue have been conducted either (a) to provide information concerning a particular problem or (b) to obtain fundamental information. In this test, it is to obtain the information regarding the crack initiation and metal changing behaviour with increasing stress level and to monitor by using FBG sensors.

When the applied stresses are low and within the elastic range of the material, the strain is directly proportional to the stress and there is either little or no difference between tests based on controlled strain or stress limits. In the case of low-cycle fatigue tests however, the applied stresses are generally high enough to cause plastic deformation and corresponding hysteresis in the stress-strain behaviour. If, in such tests, the load limits are maintained constant, the limits of deformation or strain will vary through at least some part of the life and vice versa. Therefore, low-cycle fatigue tests need to be further identified as constant-stress or constant–deformation tests. A limited number of exploratory tests controlling limits of "true" stress have been conducted by Lin and Kirsch [4]. In spite of the fact that extreme care was exercised monitoring these "true" stress limits, large scatter occurred in the test results because of the difficulty of controlling the "true" stress in low-cycle fatigue tests. There is some low-cycle fatigue tests reported in which the specimens were subjected to repeated applications of high temperature. Tests in which cyclic heat was used to introduce constant de formation ranges to the specimen have been included in this report as constant-deformation type tests [1].

### 2.1 **Optical Fiber Sensing**:

Optical fibre, being a physical medium, is subjected to animation of one kind or the other at all times. The response to external influence is deliberately enhanced in fibre optic sensing so that the resulting change in optical radiation can be used as a measure of the external perturbation. Optical Fibre when used as a transducer, converts measurements data like temperature, stress, strain, rotation or electric and magnetic currents into a corresponding change in the optical radiation. The light is characterized by amplitude (intensity), phase, frequency and polarization. Any one or more of these parameters may undergo a change when subjected external

perturbation. The usefulness of the fiber optic sensor therefore depends upon the magnitude of this change and also on the ability to measure and quantify the same reliably and accurately [5].

## 2.2 **FBG Review**

### 2.2.1 FBG

The periodic structures of gratings give them wavelength dependent properties. A grating is a repetitive array of diffracting elements (apertures or obstacles) which has the effect of producing periodic alterations in the phase, amplitude, or both of an emergent wave [6]. Group delay is an important characteristic of FBG and can be tailored for dispersion compensation. FBG has a central lobe and is mainly used in reflection.

### 2.2.2 Applications of Fiber Bragg Grating (FBG) Sensors:

Like other implementations of fibre optic sensors, the FBG is ideal for use in electrical power industry due to its immunity to electromagnetic interference. Loading of power transmission lines, winding temperature of electrical power transformers have been measured with the FBG sensor [7] [8]. For Load Monitoring of Power Transmission Lines a multiplexed FBG sensor array can be used. The load change is simply converted into strain via a metal plate attached to the line and onto which the FBG is bonded. Obviously many more sensors are required for such an application. This is an excellent example of applying FBG sensors for long-distance remote monitoring in harsh environments [7] [8]. Winding temperature measurement for defective or degraded equipment can be detected by continuously monitoring the variations in the winding temperature, which reflects the performance of the cooling system. FBG sensors are one of the best choices for this application [7] [9]. A range of miniature fiber optic sensors based on intensity modulation has been successfully commercialized in recent years for using in medicine [7] [8]. The FBG sensor can also be used for the measurement of the heart's efficiency based on the flow-directed thermo dilution catheter method in which doctors inject a cold solution into patients to measure their heart's blood output. A flow directed thermo dilution catheter is inserted into the right atrium of the heart, allowing the solution to be injected directly into the heart for measurement of the temperature of the blood in the pulmonary artery. By combining temperature readings with pulse rate, doctors can determine how much blood the heart pumps. Such a type of catheter with an FBG sensor has been used for replacement of a conventional

catheter [7] [9]. Fibre optic sensors could be ideal for applications in the oil and gas industry due to their inherent advantages, such as being intrinsically safe, immune to EMI, workable at high temperature, capable of multiplexing, and minimally invasive [7][8]. FBG sensors can be used in pipeline in order to monitor the temperature in the pipe or the pressure on the joins. Because refractive index of these fibre is sensitive to pressure and temperature, one can monitor all the length of the pipe by one fibre by using multiplexing methods [7] [8].

### 2.2.3 Power Reflectivity Spectrum

The operation of FBG depends on the reflection of light from grating fringes and coupling of the modes. In a single mode FBG, the coupling occurs between the forward and backward propagating fields of the same mode. The maximum reflectivity is obtained at the wavelength providing the Bragg condition [10].

$$\lambda_B = 2n_{eff}\,\Lambda \quad \ldots\ldots\ldots \quad (1)$$

Here, $n_{eff}$, $\Lambda$ and $\lambda_B$ , represent the effective refractive index of the core, grating period and Bragg wavelength, respectively. A uniform Bragg grating has a constant grating period. The optical characteristics of a FBG can be determined from its reflectivity spectrum, which shows the wavelength range of operation and bandwidth. The reflectivity spectrum of the grating can be calculated numerically using matrix transfer method [10]. In Figure 1, the power reflectivity spectrum of uniform FBG with a 10 mm length is shown for different index difference ($\delta\, n_{eff}$) values.

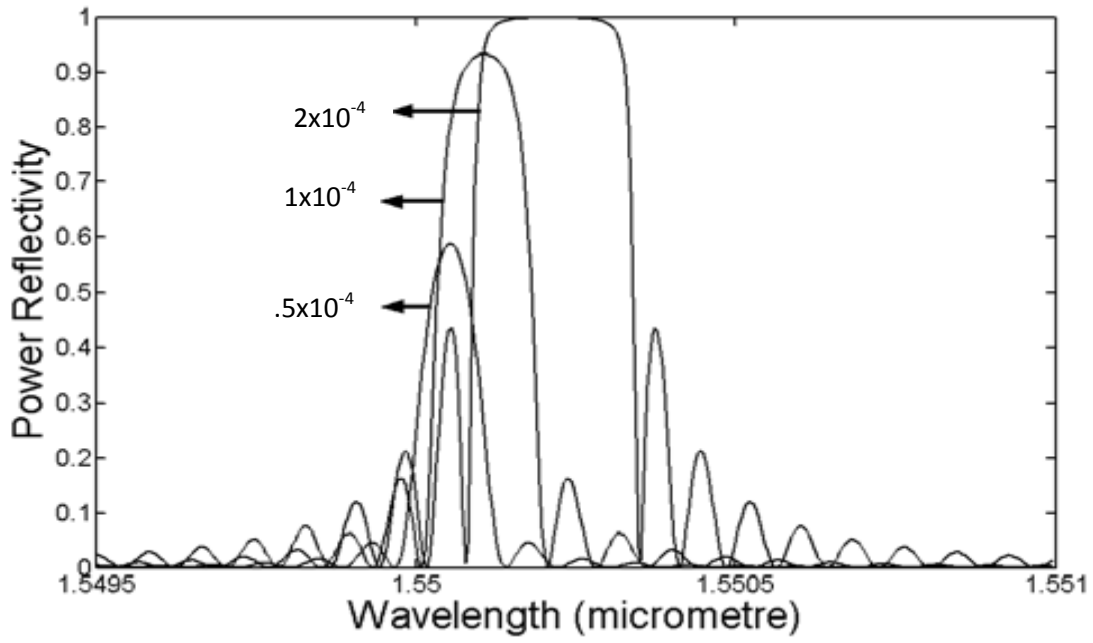


Fiugre1, Power reflectivity spectrum of uniform fibre reflection gratings (From reference 14, Section III.)

Increasing the chirp parameter broadens the reflection spectrum but decreases the reflectivity power for a certain grating length. On the other hand, if the grating length increases, group delay of the reflection band and therefore dispersion compensated bandwidth increases [10].

### 2.2.4 Strain Sensitivity of FBG:

The strain sensitivity is caused by the physical elongation of the FBG period and photo elastic effects. The effective refractive index ($neff_)$ and the grating period ($\Lambda$) are important factors in determining the wavelength of the FBG. Both factors are very sensitive to ambient changes; therefore, the central wavelength is left tunable in terms of strain, temperature, pressure, voltage, magnetic field etc. The stretching or the compression of the fiber changes the grating period, and the refractive index which changes the central wavelength of the FBG by increasing or decreasing its value. When the FBG is subjected to disturbance like strain, the change in the central wavelength can be found by a partial differentiation of the central wavelength with respect to the length taken that the effect of temperature is discarded. The strain sensitivity of typical FBG sensors is between 1 to 5 με determined by the accuracy of the wavelength measurement of the instrument used.

## 2.3 **Stress Concentration**

A stress concentration is formed when there is a discontinuity in the geometry, structure, or temperature in a material although the term "stress concentration" generally refers to the stress increase resulting from a notch in a member. According to the elasticity theory, *a stress concentration factor*, which is the ratio of the maximum stress to the nominal stress in the member, can be computed for most types of notches. *Another stress factor* which is used in fatigue studies is the "effective stress concentration factor", defined as the ratio of the fatigue strength of an un-notched specimen to that of a notched specimen. At the present time, the effective stress concentration factor can only be obtained by experimental means [4].

A great amount of effort has been devoted to studies of the effects of stress concentrations in fatigue. It is generally found that the material in the region near a stress concentration deforms plastically in most fatigue tests. This is especially true in low-cycle fatigue tests where the applied stresses are high. This yielding affects the stress concentration in the way of:

(a) The ratio of the maximum stress to the average stress is no longer a constant; and

(b) The geometry of the notch, which is the basis for the calculation of the theoretical stress concentration changes.

In addition, work hardening is generally introduced in the vicinity of the tip of the notch, and a new complication results from the non-uniformity of the material. Consequently, the theoretical stress concentration factor for a notched specimen becomes a fictitious quantity when, yielding of the material occurs at the notch. However, since it is desirable to use numerical values in representing the severity of various notches, the theoretical stress concentration factor is often useful for purposes of comparison [4].

## 2.4 **Extent and Rate of Cyclic Hardening and Softening**

In cyclic stress controlled fatigue test, the stress is held constant during cycling. The stress-strain response during cycling can change; as plastic deformation is not completely reversible though elastic strain is reversible. The metal can undergo cyclic strain hardening or cyclic strain softening, or remain stable [11].

By recording strain variation as function of cycle character of the material can be analyzed. Hardening indicates increased resistance to deformation and the plastic region of the loop reduced with pronounced hardening characteristics of the sample. On the other hand, softening

indicates decreased resistance to deformation and the plastic region was expanded and the hysteresis loop area was enlarged.

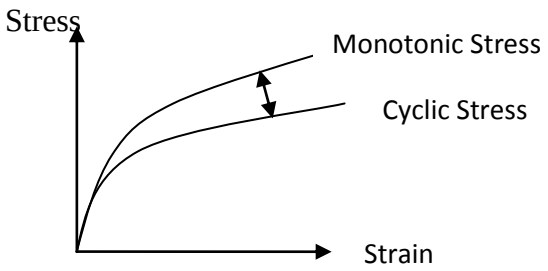


Figure 2 (a) Cyclic Softening

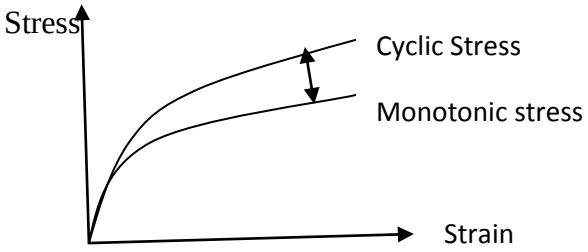


Figure 2(b) Cyclic Hardening

Deformation can be observed according to cyclic stress- strain curves from figure 2(a) and 2(b)

(a) *Cyclic Softening*: When a material cyclically softens, the cyclic stress is considerably lower than the monotonic yield stress.

(b) *Cyclic Hardening*: During cyclic hardening of the material, the yield stress is higher than the monotonic yield stress .When considerable plastic strains are present; by applying monotonic properties the elastic strain can be predicted. In general, metals with high monotonic strain exponents undergo cyclic hardening and with low strain hardening exponents undergo cyclic softening. Determining metal behavior cyclically was proposed by Smith et al [12] and expressed as: If the ratio of tensile strength $S_u$ and yield strength $S_y$ is greater than 1.4 then hardening is expected.

$$S_u/S_{0.2\%y} > 1.4 \qquad (1)$$

On the other hand if this ratio is less than 1.2 then cyclic softening is to be expected and expressed as,

$$S_u / S_{0.2\%y} < 1.2 \qquad (2)$$

## 2.5 **Study of Hysteresis**

Area within a hysteresis loop is energy dissipated during a cycle. It represents plastic work from the cycle. Change in deformation behavior, is more at the beginning of cyclic loading and then gradually stabilizes with continued cycling. A transition from cyclic hardening response to cyclic softening response with increasing applied plastic strain amplitudes or increasing cyclic stress amplitudes can be observed in many of the cases with technical purity of aluminum alloys [13]. It is worth mentioning that Kunz *et al*. [13] [14] have reported that cyclic softening, is observed

in strain controlled tests, whereas load controlled tests generally yield cyclic hardening or cyclic saturation response. According to some experts, both strain controlled and load controlled tests can detect cycle hardening, cyclic softening, and cyclic stabilization. However, the cyclic plastic strain imposed on to the samples are lower in many of the reported stress controlled tests [13-14-15] compared to that of the strain controlled tests [13] [16]. As such, the observation of cyclic softening only in the case of strain controlled tests and cyclic hardening/saturation in the load controlled tests reported in [13] [16]. It should be noted that in some cases for aluminum alloys, the cyclic softening response is preceded by a cyclic hardening response [13] [17-18].

### 2.6 **Fatigue crack initiation, propagation and ultimate failure study**

Fatigue Crack Propagation: Linear elastic fracture mechanics assumes that all structures contain flaws. Cracks grow from an initial size to a critical size corresponding to failure as a function of the number of load cycles .The crack growth rate can be determined from the PSA slope of the curve. Initially, crack growth rate is slow but increases with increasing crack length and of course, the crack growth rate is also higher for higher applied stresses [19].

Stress Relief Cracking (Stress relaxation): Reheat cracking is kind of inter granular cracking in the HAZ or weld metal occurs during the stress relief heat treatment or during service at high temperature [20]. According to Tiawen Zhao et al. [23] materials of different types exhibit different fatigue cracking behavior in the transient zone after an overload is applied. Most materials show, the crack growth rate first from to a minimum value and then increases rapidly to the stable value under constant amplitude loading. Some material corresponds to an acceleration of the crack growth rate immediately after overloading [23]. A high overload can also result in the arrest of crack growth.

From scholarly articles and especially from reference [19-25] it is learnt that fatigue is a problem that can affect any part or component that moves. Basic factors necessary to cause fatigue are: (a) a maximum tensile stress of sufficiently high value, (b) a large enough variation or fluctuation in the applied stress, and (c) a sufficiently large number of cycles of the applied stress. The fatigue strain-life curve tends toward the plastic curve at large strain amplitudes and toward the elastic curve at small strain amplitudes. Fatigue crack nucleation and growth occurs in the following stages.

(i) Stage I: Crack initiation usually starts at a notch or other surface discontinuity. Even in the absence of a surface defect, crack initiation will eventually occur due to the formation of persistent slip bands (PSBs), which are a result of the systematic buildup of fine slip movements. The back-and-forth movement of the slip bands leads to the formation of intrusions and extrusions at the surface, eventually leading to the formation of a crack. The initial crack propagation rate during stage I was very low, and produce a practically featureless fracture surface. The crack initially follows the slip bands at approximately $45^0$ to the principal stress direction. When the crack length becomes sufficient for the stress field at the tip to become dominant, the overall crack plane changes and becomes perpendicular to the principal stress, and the crack enters stage II.

(ii) Stage II: Crack growth occurs when the stage I crack changes direction and propagates in a direction normal to the applied stress. Crack growth proceeds by a continual process of crack sharpening followed by blunting. Frequently, visible examination of a fatigued surface will reveal a series of concentric markings on the surface, which is referred to as beach marks .These are present as a result of stress changes during fatigue [11].

(iii) Stage III: Ultimate failure occurs when the fatigue crack becomes long enough that the remaining cross section can no longer support the applied load. Finally, in region III, the crack growth rate accelerates, since the fracture toughness of the material is approached, and there is a local tensile overload failure [11].

## 2.7 **Significant Contribution of the Thesis**

During the experiment three FBG sensors were surface mounted on the top side of all the FSW AA2219 aluminum alloy samples in order to monitor the onset of crack initiation and the behavior of metal specified zones (Nugget, Heated and Thermo-mechanical affected). Effort was made to obtain high quality bonding strength and with the flat cladding FBG sensors strain amplitude of up to ±11000με was reached. Significant changes of plastic strain amplitude (PSA) slope was observed in the last few cycles which corresponds to metal crack initiation, propagation and the ultimate failure.

## 2.8 **Outline of the thesis**

Chapter 2: **FBG Sensors distribution, FSW Sample Study and its strain Behavior**, this chapter explains, FBG sensors distribution, parameters and FSW Al alloy specimen. Also describes about tensile properties and Strain hardening behavior of FS Welded AA2219 Al alloy.

Chapter 3: **Bonding and Experiment**, the bonding procedure of FBG array on substrate and the experiment sequential steps are described in this chapter.

Chapter 4: **Experimental Results and Discussions**, this Chapter presents experimental results and discusses the details of the analysis and the observations from the experiments conducted on different sample types.

Chapter 5: **Conclusion and Future work**, the closure discusses the final remarks regards to the experimental works as well as the improvements for further study.

**Chapter 2**

## 3. Flat clad FBG sensors parameters and locations

### 3.1 Localized FBG Sensors on FS Welded sample 3B24:

On top surface of sample number 3B24 three FBG sensors are surface bonded. The distance between the sensors are 7.5 mm and the sensor1 is placed at 5mm away from the blue mark as shown in figure 3(a). The FBG parameters are:

- Series number : 0112-$A_1$
- Wavelength: $\lambda_1$= 1541.312 nm, $\lambda_2$ =1547.488 nm, $\lambda_3$= 1553.904 nm
- Transmission :T = 7.09 dB ($\lambda_1$), 6.93 dB ($\lambda_{2)}$, 7.33 dB ($\lambda_3$)
- Full-width at half maxima; $\Delta\lambda$ = 0.460 ($\lambda_1$), 0.432 ($\lambda_2$), 0.528 ($\lambda_3$)
- Sensor length = 4 mm, total length of a SINC function
- Sensors are labeled as sensor #1(S1), Sensor #2(S2) and Sensor # (S3).
- Three lines in figure 3(a) at sensor position indicate the location of the grating and its masking center with the middle line.
- Blue mark on fiber coating: Used as reference point to identify location of the first sensors.
- Break Point: It is mentioned in the figure as it is the ultimate macro crack point.

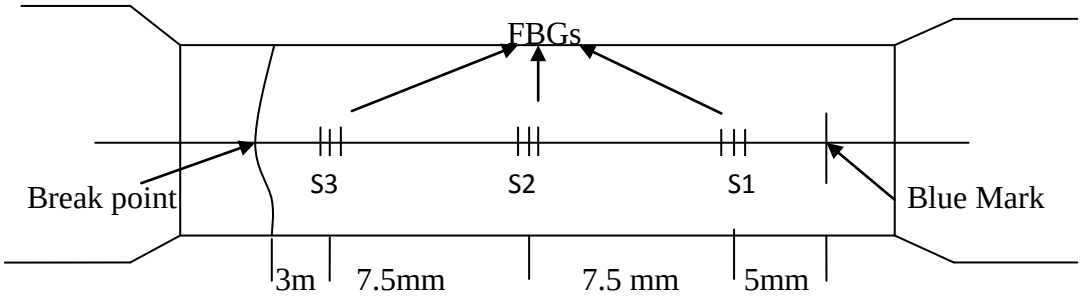


Figure 3(a), FBG array sensors distribution on Aluminum alloy of sample 3B24

### 3.2 Localized FBG Sensors on FS Welded sample 2T25

On top surface of sample number 2T25 FBG Sensors are also surface bonded. The distance between the sensors are 7 mm and sensor1 at 5mm away from the blue mark, as shown in figure 3(b). The FBG parameters are:

- Series number : 0425-$A_1$

- Wavelength: $\lambda_1$= 1530.50 nm, $\lambda_2$ =1539.750 nm, $\lambda_3$= 1551.150 nm
- Transmission(T) = 6.07 dB ($\lambda_1$), 5.67 dB ($\lambda_{2)}$, 6.46 dB ($\lambda_3$)
- Sensor Length = 4 mm

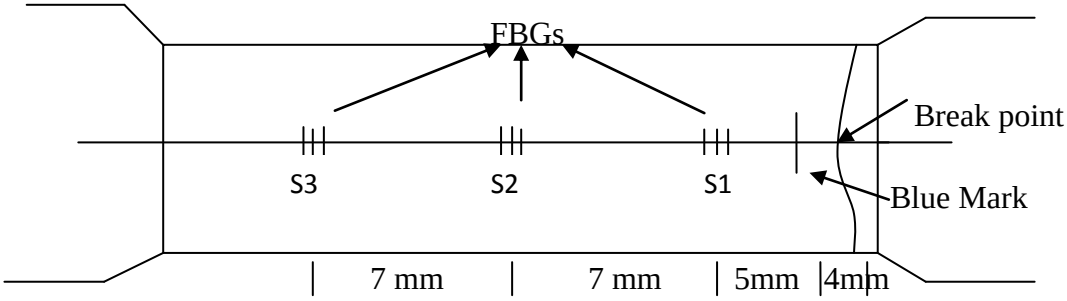


Figure 3(b), FBG array sensors distribution on Aluminum alloy of sample 2T25

3.3 **Aluminum alloy sample material study**:

3.3.1 LCF Specimen:

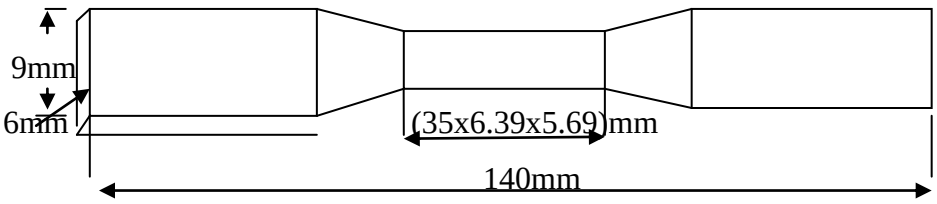


Figure 4, Sample of aluminum alloy

Figure 4, shows the dimensions of the fatigue test samples. There were 8 pieces of friction stir welded AA2219 Aluminum alloy for testing. The size of the specimen was 140 mm x 9mm x 6mm and the gauge section was 35mm x6.39mm x 5.69mm, which was machined perpendicular to the FSW direction. There are four zones in this 35 mm long section, namely, nugget zone (NZ), thermo mechanically affected zone (TMAZ), heat affected zone (HAZ) and base metal. The FBG sensors, each having a length of 4 mm were surface mounted in the centre of NZ and across TMAZ and NZ.

3.3.2 Friction Stir Welding (FSW):

Structural application of Al alloys involve welding and joining, which are challenging using conventional fusion welding processes. Therefore, robust joining techniques are required to expand the applications of Al alloys. Friction stir welding (FSW), which was invented by The Welding Institute (TWI) of UK [26-1], provides a promising solution since it is an environment-friendly and energy-effective solid-state joining technique. This offers significant benefits over conventional joining processes due to the absence of the fusion zone [26-4]. This joining technique has been proven to be one of the good alternatives especially for the lightweight aerospace materials such as 2xxx-series aluminum alloys.

3.3.3 Friction Stir Welded AA2219 Al Alloy Material: The nominal of AA2219-T62 aluminum alloy plate has the chemical composition [26] of following:

Table 1: Chemical composition (wt %):

| Cu | Mn | Fe | Ti | V | Zn | Si | Zr |
|---|---|---|---|---|---|---|---|
| 6.48 | 0.32 | 0.23 | 0.06 | 0.08 | 0.04 | 0.49 | 0.2 and Balance Al |

Before FSW, the surface oxides were removed and then cleaned using ethanol. The FSW tool had a shoulder of 34 mm in diameter and a threaded (left-handed screw) cone-shaped pin of 13.5 mm in root diameter and 9.3 mm in tip diameter, and was rotated clockwise [26]. With a tool rotational rate at 300 rpm and traverse/welding speed of 80 mm/min the FSW was performed. The tilt angle of rotational tool was set to 2.8° with respect to Z-axis of FSW machine [27]. Cooling water was sprayed onto the welding tool and on the top surface of weld. The cross section of the welded joint was ground with water abrasive papers, and then polished using diamond paste up to 1 μ m [26].It was then etched with Keller's reagent (1 ml hydrofluoric acid, 1.5 ml hydrochloric acid, 2.5 ml nitric acid and 95 ml distilled water), then the microstructure was examined using a light microscope in conjunction with an image analysis system [26]. Sub-sized tensile specimens with a gauge length of 35 mm (i.e., a parallel length of 32mm) and width of 6 mm in accordance with ASTM E8M standards, were cut perpendicularly to the welding directions (or the rolling direction for the base material) and sliced equally into three pieces (top, middle and bottom) in the thickness direction, and then machined to the required dimensions

using the electro-discharge wire cutting [26]. The gauge area of specimens was ground with SiC papers up to grit 600 along the loading axis to get rid of the cutting marks and to achieve a smooth surface [26]

3.3.4 Tensile properties and strain hardening behavior of FS W AA2219 Al Alloy:

Strain-hardening behavior is one of the important considerations in the evolution of plastic deformation of materials [26-5,6], thus numerous investigations in this aspect have been conducted. For example, strain hardening of ultrafine-grained copper with nano scale twins was studied by Chen and Lu [26-6]. Afrin *et al*. [26-7] reported that the hardening capacity and the strain hardening exponent of a friction stir welded (FSW) magnesium alloy were about twice and threefold higher than that of the base alloy. A novel microstructure-based strain-hardening model for a precipitate-hardened aluminum alloy 6005A-T6 after FSW was developed by Simar *et al*. [26-8]. The main changes in the tensile properties of the welds were explained via the differences in the strain-hardening behavior which controlled the strength and resistance to plastic localization. In particular, the lower strength in the heat-affected zone (HAZ) compared with the weld nugget zone (NZ).

## Chapter 3

## 4. Experiments

### 4.1 FBG Bonding Procedure on Substrate

4.1.1 Tools used for Bonding:

Sample, Sand papers (320,600, LPA12), Flat clad fiber grating, Glue, Foil paper, Blue tape, Scissor, Knife, Marker, Weight, Rubber sheet, scale, Alcohol, Aluminum foil tape , a piece of stripped out fiber to put glue on substrate, Non-stick paper, Calculator, Micrometer and Non-stick metal tray, a table /chart to keep information of substrate FBG sensors and test information: this table should have the file name relating substrate number, test date and particular MPa.

4.1.2 Bonding Steps:

(a) Grinding and Cleaning: ground the sample using sand paper 320, and aluminum oxide LPA 12 micron at $90^{o}$ and clean with Gasoline and alcohol.

(b) Glue Preparation: Prepare epoxy glue (9:1) and preserve in refrigerator. For example, [Epoxy 353ND (part A) = 9 and hardener (part B) =1. If epoxy weights 1.3746 gm, the hardener will be 1.374/9= 0.1527 gm and total mixture will be (1.3746+0.1527= 1.5273gm)].

(c) Procedure: Before using glue, measure sample cross section (width and thickness at three points and considering the one with small value) for applying stress data during fatigue test. Mark the substrate with corresponding measurements of fiber grating. Mark the sample both side (keeping 70 mm approximately in the center) and fix it with fatigue test fixture machine at mechanical lab. Place the flat clad fiber grating keeping marked end at the right side. To confirm the alignment of the fiber with the facet facing up, check it under microscope. Then tape two aluminum foils on the substrate to form a trench with the fiber sensors in the middle to confine the epoxy. Put a thin layer of glue uniformly without any bubble and place a non stick transparent paper or thin film paper (which is used to cover the display of cellular telephone set) on the glue or cover with yellow plain rubber sheet (when non-stick paper is used). Put weight covering all sensors to ensure a good contact between the fiber and substrate.

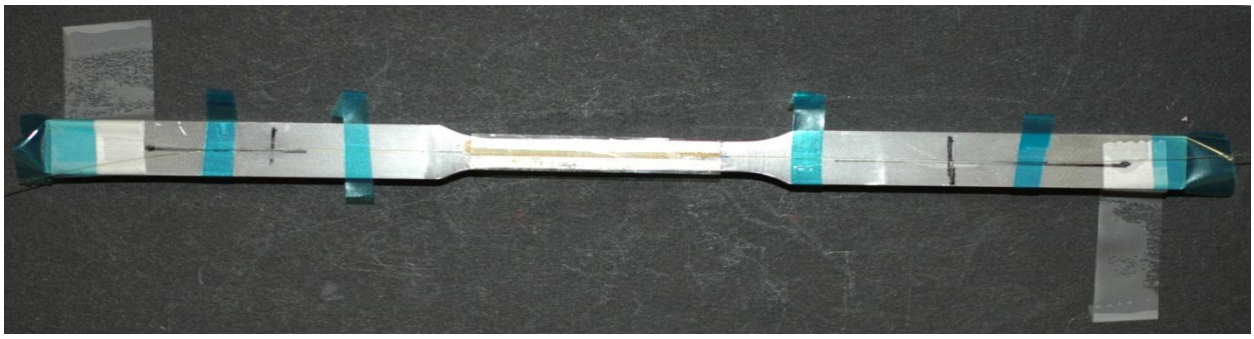

Figure 5, FBG array bonded Al alloy sample

(d) Curing: Preheat oven at $80^{o}$ centigrade for 25 minutes and then place the assembly in the oven for epoxy curing for 45 minutes.

### 4.2 **Instrument and Procedure**

4.2.1 Instruments used during test:

(a) Lap Top (connected to a data acquisition card and a Si 425 interrogator) to monitor strain variation and store test data.

(b) Data Acquisition card, USB 620 of National Instruments- To convert stress signal (from output port of the Instron system computer in volts) into digital signal that would be saved in the Lap Top.

(c) OSA (Optical Spectrum Analyzer), ANDO. AQ6331 -To record FBG sensor spectra

(d) INSTRON ((to conduct fatigue tests)

(e) FBG Interrogator Si 425 (to record FBG peak wavelengths as a function of time)

(f) USB to save the test raw data.

(g) Bonded samples.

(h) Circulator (To measure the reflection spectra of sensors)

4.2.2 Schematic Diagram of Testing System:

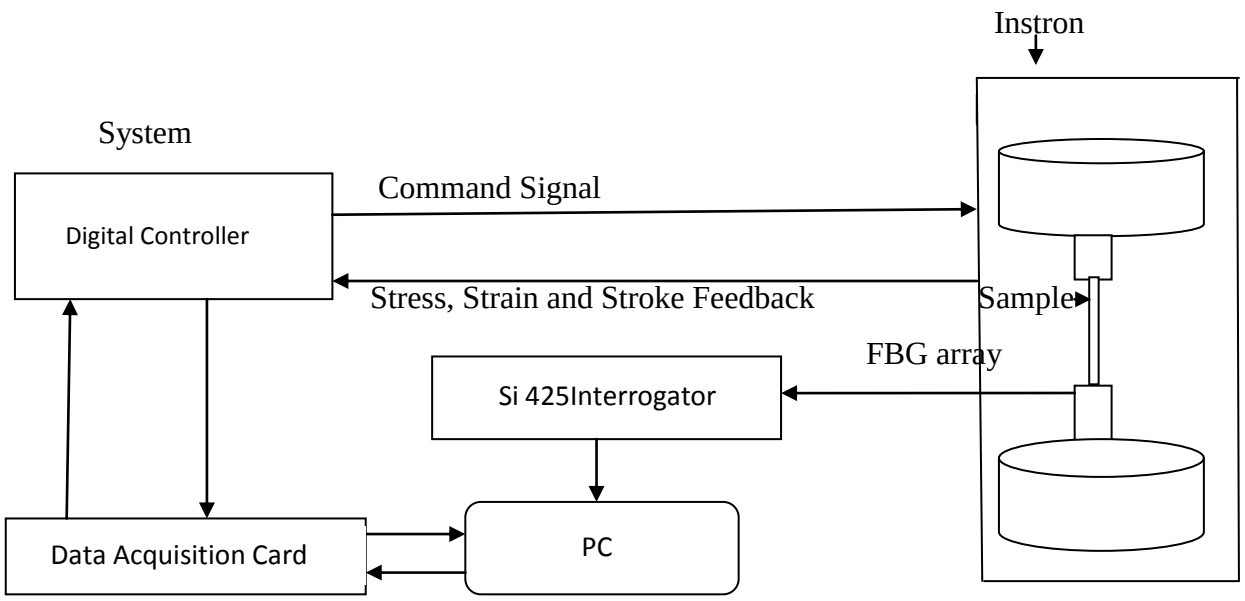


Figure 6, Schematic Diagram of Fatigue Testing System

Instron 8801 servo hydraulic testing system provided complete testing solutions and is ideally suited for high and low cycle fatigue testing, thermo-mechanical fatigue testing, and fracture mechanics. The precision mechanical system is combined with advanced features of 8800 digital controller. Console software of the Instron controller provides full system control from a PC: waveform generation, calibration, limit set up, and status monitoring. Analog controller output from port B, collected through a data acquisition card (National Instruments, Ni USB620), digitized and fed to the computer. Another set of data from Si425 FBG interrogator (Optical Sensing Interrogator of Micron Optics Inc.) was recorded simultaneously with stress signals from Instron system.

4.2.3 Instruments set up of Testing System (Interconnections):

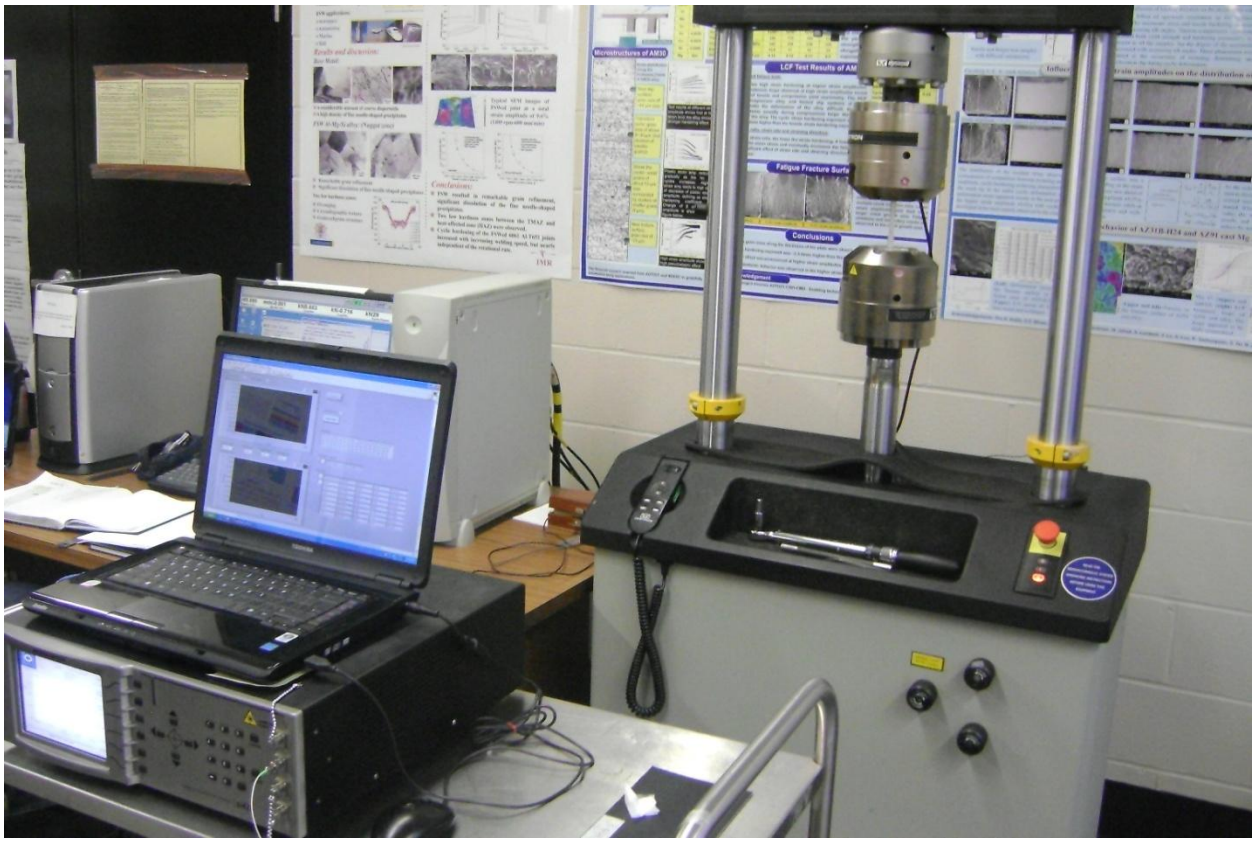

Figure 7, a photo of Instron Controller 8801 fatigue Testing System

- INSTRON fast track 8800D back side port B (output) to data acquisition card (Ni USB 620) and other end of data capture card to laptop (left).
- Si425 back side port with green cable to PC/laptop left side USB port.
- PNC between channel port of Si425 and one end of substrate sample.
- Other end of sample with load controller.

4.2.4 OSA Spectra recording Steps:

- Port 1 of circulator connected to broadband light source
- Port 2 of circulator with APC connected to the FBG.
- Port 3 of circulator connected to the input of OSA
- Switch ON OSA

- Press sweep button of OSA
- Press scan button of OSA
- Spectrum of FBG sensors in db level will be displayed.

4.2.5 Steps to save stress data:

- Sequence has to be followed to save test data: must discuss with INSTRON operator about saving data procedure for future analysis and reference.
- Check the active channel with OSA and your PC which should be same.
- Click 'ON'- at the left of active channel
- Give the file name as per your prepared table
- Press OK
- Once INSTRON controller is ready (Talk to Other operator of INSTRON)
- Press 'Save Data'
- Then INSTRON controller operator to press 'OK'
- Sharp at $100^{th}$ cycle of every MPa click 'Saving Data" box
- Then Stop.
- Tested (acquired) data to be preserved for analysis.

## 4.3 **Fatigue Test of FS Welded Al alloy AA2219**

### 4.3.1 Low cycle Fatigue:

Low- cycle fatigue is when the number of cycles to failure is small (typically the number of cycles to failure, $N_f$, is less than 1000 and high-cycle fatigue is when the number of cycles to failure is large (typically the number of cycles to failure, $N_f$ is greater than 1000). The data evaluation of low-cycle fatigue of metal depends on the type of test, cyclic rate, stress concentration, crack propagation, material property change, and method of analysis. Low-cycle fatigue tests subject specimen to repeated stress or strain until failure occurs at a relatively small number of cycles. Some investigator has generally selected the upper limit of lower cycle life in the range of $10^4$ to $10^5$ cycles; but to some investigator, the lower limit of life cycle is below approximately $10^4$ [22] [1]. Low cycle fatigue is relevant to the structures where at high stress and at low number of cycles the failure occurs. For example, the power generator structures that operates at an elevated temperature and faces significant stresses. The microscopic plastic

deformation occurs at low cycle fatigue. But in view of high stress level, final failure will occur even when the cracks are still small [1].

4.3.2 Stress Control fatigue testing procedure: A closed loop servo hydraulic axial load frame is used to conduct the test, where the test system uses the stress output to provide feedback to the servo controller. Figure 6 and figure 7 are the stress and strain controlled fatigue testing system's schematic diagram and photo respectively. The push pull type fatigue tests were carried out using a computer controlled Instron fatigue testing system (Instron Fast Track 8800, Norwood. MA).

- A triangular waveform of stress signal was applied at a constant stress rate of 25 MPa increment. The substrate sample was tested for 100 cycles in each stress level, starting from 50 MPa until failure.
- During this Low Cycle Fatigue (LCF) tests the wavelength shifts of FBGs were recorded by interrogator (Si 425, Micron Optics). Then this shift was converted to strain.
- The applied load (stress value) was known and strain and stress values were recorded as a function of time for each fatigue cycle.

## Chapter 4

## 5. Experiment Result Evaluation

### 5.1 Fatigue Load table:

Table 2: Load table:

| **Sample ID: 3B24 Cross Section: 36.19 (mm)$^2$** | | | | | | | | | | |
|---|---|---|---|---|---|---|---|---|---|---|
| | | **1st Test** (Compression) | | **2nd Test** (Tensile) | | **3rd Test** (Neutral) | | **4th Test** (Fatigue) | | |
| Stress (MPa) | Load (kN) | Amplitude | Set pt(kN) | Amplitude | Set Pt(kN) | Amplitude | Set pt(kN) | Amplitude | Set Pt | # cycles |
| 50 | 1.810 | 0 | -1.810 | 0 | 1.810 | 0 | 0 | 1.810 | 0 | 100 |
| 75 | 2.714 | 0 | -2.714 | 0 | 2.714 | 0 | 0 | 2.714 | 0 | 100 |
| 100 | 3.619 | 0 | -3.619 | 0 | 3.619 | 0 | 0 | 3.619 | 0 | 100 |
| 125 | 4.524 | 0 | -4.524 | 0 | 4.524 | 0 | 0 | 4.524 | 0 | 100 |
| 150 | 5.429 | 0 | -5.429 | 0 | 5.429 | 0 | 0 | 5.429 | 0 | 100 |
| 175 | 6.333 | 0 | -6.333 | 0 | 6.333 | 0 | 0 | 6.333 | 0 | 100 |
| 200 | 7.238 | 0 | -7.238 | 0 | 7.238 | 0 | 0 | 7.238 | 0 | 100 |
| 225 | 8.143 | 0 | -8.143 | 0 | 8.143 | 0 | 0 | 8.143 | 0 | 100 |
| 250 | 9.048 | 0 | -9.048 | 0 | 9.048 | 0 | 0 | 9.048 | 0 | 100 |
| 275 | 9.952 | 0 | -9.952 | 0 | 9.952 | 0 | 0 | 9.952 | 0 | 50 (failed) |
| **Sample ID : 2T25 Cross Section: 34.054 (mm)$^2$** | | | | | | | | | | |
| | | **1st Test** (Compression) | | **2nd Test** (Tensile) | | **3rd Test** (Neutral) | | **4th Test** (Fatigue) | | |
| Stress (MPa) | Load (kN) | Amplitude | Set pt(kN) | Amplitude | Set Pt(kN) | Amplitude | Set pt(kN) | Amplitude | Set Pt | # cycles |
| 100 | 3.405 | 0 | -3.405 | 0 | 3.405 | 0 | 0 | 3.405 | 0 | 100 |
| 125 | 4.257 | 0 | -4.257 | 0 | 4.257 | 0 | 0 | 4.257 | 0 | 100 |
| 150 | 5.108 | 0 | -5.108 | 0 | 5.108 | 0 | 0 | 5.108 | 0 | 100 |
| 175 | 5.959 | 0 | -5.959 | 0 | 5.959 | 0 | 0 | 5.959 | 0 | 100 |
| 200 | 6.811 | 0 | -6.811 | 0 | 6.811 | 0 | 0 | 6.811 | 0 | 100 |
| 225 | 7.662 | 0 | -7.662 | 0 | 7.662 | 0 | 0 | 7.662 | 0 | 100 |
| 250 | 8.514 | 0 | -8.514 | 0 | 8.514 | 0 | 0 | 8.514 | 0 | 100 |
| 275 | 9.365 | 0 | -9.365 | 0 | 9.365 | 0 | 0 | 9.365 | 0 | 100 |
| 300 | 10.216 | 0 | -10.216 | 0 | 10.216 | 0 | 0 | 10.216 | 0 | 34 (failed) |

In experiments, the cyclic stress was applied from 50 MPa which continued till 275 MPa or 300 MPa for two samples respectively with a 25 MPa increment. The failure at 275 MPa for FSW sample 3B24 and at 300 MPa for sample 2T25 were observed.

## 5.2 **Corresponding behavior with a previous researcher**

(Strain controlled LCF Test) by C. Li, "The Fiber Optic Sensing array for Fatigue LCF Tests", [28] where it was observed:

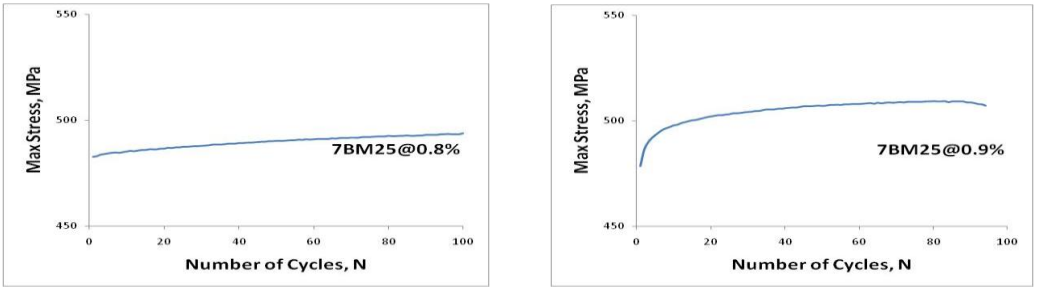


Figure 8(a) at cyclic strain level of 0.8%, 8(b) at cyclic strain level of 0.9% of sample7Bm25

Plot represents maximum stress from 1st cycle to 100th cycle at cyclic strain amplitude of 0.8% and 0.9% respectively. The maximum stress at cyclic strain amplitude of 0.8% increased from 482.66 MPa at 1st cycle to 493.97 MPa at 100th cycle. However, at cyclic strain amplitude of 0.9%, the maximum stress started from 478.59 MPa, reaching its highest value of 509.34 at 83th cycle, then decreased to 507.23 MPa at **94th** cycle when it was broken.

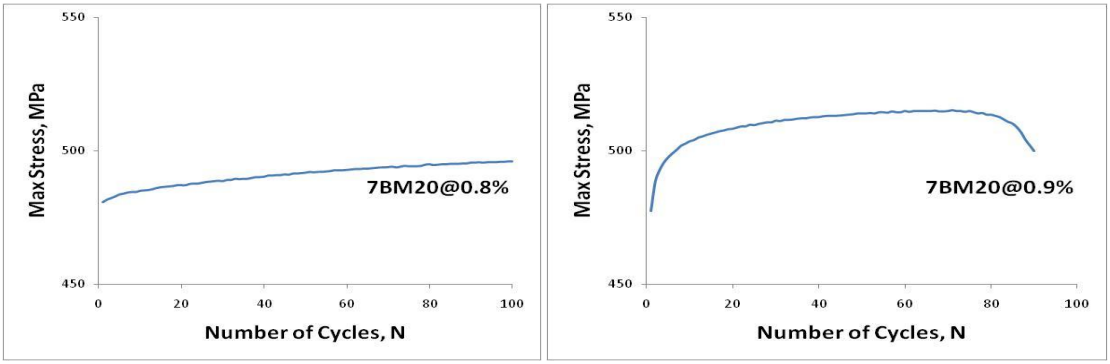


Figure 9(a) at cyclic strain level of 0.8%, 9(b) at cyclic strain level of 0.9% of sample 7BM20

Plot represents maximum stress from 1st cycle to 100th cycle at cyclic strain amplitude of 0.8% and 0.9% respectively. At cyclic strain amplitude of 0.8%, the maximum stress increased monotonously from 480.73 MPa at 1st cycle to 495.93 MPa at 100th cycle.

Comparing with the 7BM25, the same trend was observed at cyclic strain amplitude of 0.9%, the maximum stress started from 477.57 MPa, reaching maximum of 515.19 at 71th cycle, then

decreased to 499.99 MPa until it was broken. This sample was broken at **$90^{th}$** cycle of cyclic strain amplitude of 0.9%

In view of the experiment result I have also observed the identical behavior of the material with C. Li's experiment, especially the significant changes happen at last few cycles with highest stress level before the ultimate crack. Sample 3B24 broke at $50^{th}$ cycle at 275 MPa and the significant change was observed between $40^{th}$ cycles to $50^{th}$ cycle. Sample 2T25 broke at $34^{th}$ cycle at 300 MPa stress level and plastic strain amplitude slope changing between $25^{th}$ cycles to $34^{th}$ cycle. These will be verified with my experiment result and plotting in subsequent sections.

## 5.3 Study of Crack Initiation and Propagation

The PM (Philosophical Magazine) theory on crack propagation, originally developed for long-life fatigue tests, was expanded by Head [29] to include the low-cycle range of fatigue tests. The theory, based on an idealized material and consisting of elastic, elastic-shear and fully plastic elements, indicates that

(a) Cracks may initiate at an early stages of fatigue test,

(b)The inverse square-root of crack length is a linear function of the number of cycles,

(c)The slope of the straight line (square root of the crack length versus number of cycles) is a function of magnitude of the applied stresses.

However, at present, there is little or no experimental evidence available to support this theory in the low-cycle field. McClintock [30] found that, at high strain amplitudes:

(a) Cracks always tend to grow toward the center of the remaining section: that is, "the point most distant from the boundaries".

(b) The crack propagation depended upon the integrated absolute strain increments regardless of time, number of cycles and cyclic strain increments,

(c) Cracks propagate faster in the larger of any two geometrically similar specimens under the same nominal strain amplitude,

In this experiment, specimens of Friction Stir Welded AA219-T62-T6 aluminum alloy were subjected to a selected number of cycles to examine the deformation behaviour and for crack initiation detection. From the number of tests conducted, it appears that the theoretical hypotheses mentioned above are in general accord with the experimental result. From the test

cracking initiated and the characteristics of crack growth were studied. In the test sample three sections like crack initiation, crack propagation, and the ultimate failure were observed.

This is further explained in subsequent sections with plastic strain amplitude (PSA) and different strain values as a function of fatigue cycles at different applied stress level. In the following table the sections are mentioned:

Table 3: Summary of Metallurgical Evaluation of Test Specimens #3B24 and 2T25

| **Al- alloy sample Detail** | **Findings** |
|---|---|
| # 3B24(Bottom slice)is the one from series 24 | Low Cycle Fatigue (LCF) crack initiation at the heated zone which is close to boundary started initiation about $41^{st}$ cycle and the failure occurred 3mm away from sensor #3 and 10.5 mm from $S_2$ at $50^{th}$ cycle of 275 MPa stress and the sample was ultimately broken into two pieces, [Figure 3(a), figure10(a) and later justified with fig. 14(b)] |
| # 2T25 (Top slice) is the one from series 25. | Crack initiation started occurring at the beginning of the cycle where slope goes upward($1^{st}$ - $5^{th}$ cycle) showing softening (crack initiation), then ($6^{th}$ -$24^{th}$ cycle)it is reducing linearly showing hardening (crack propagation)and after that changing slope up mean softening and then hardening ( rapid crack growth) between $27^{th}$ cycle to $34^{th}$ cycle. The crack was 16mm away from $S_2$ .It was broken into two pieces at $34^{th}$ cycle of 300 MPa stress level, [figure 3(b) ,figure 10(b)and later justified with fig. 14(g)] |


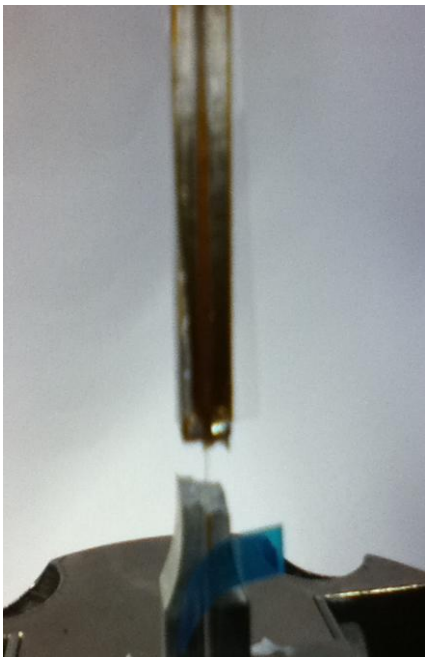

Figure 10(a) and 10(b), photos of cracked samples at $50^{th}$ & $34^{th}$ cycle respectively

5.4 **Strain Behavior of FBG sensors**:

5.4.1 **Sample 3B24**: Strain curve as a function of time for three sensors plotted as shown below:

At 250 MPa for sample 3B24 the deformation was less and at 275MPa only sensors 2 sustained which was placed in the NZ. The bonding strength of sensors (S1, S3) at the edges were not as strong as S2, which is at the center; this could also be an issue to break these sensors at this stage. In NZ, the material did not deform as much a sin the HZ and TMAZ, and the FBG bonding remains stable. By observing figure 11(a) and 11(b) for $S_2$ at 250 MPa, the strain as a function of time shows large strain amplitude at the beginning and decreases towards the end cycles. At 275 MPa due to more deformation of FSW aluminum the strain amplitude was different at many cycle points.

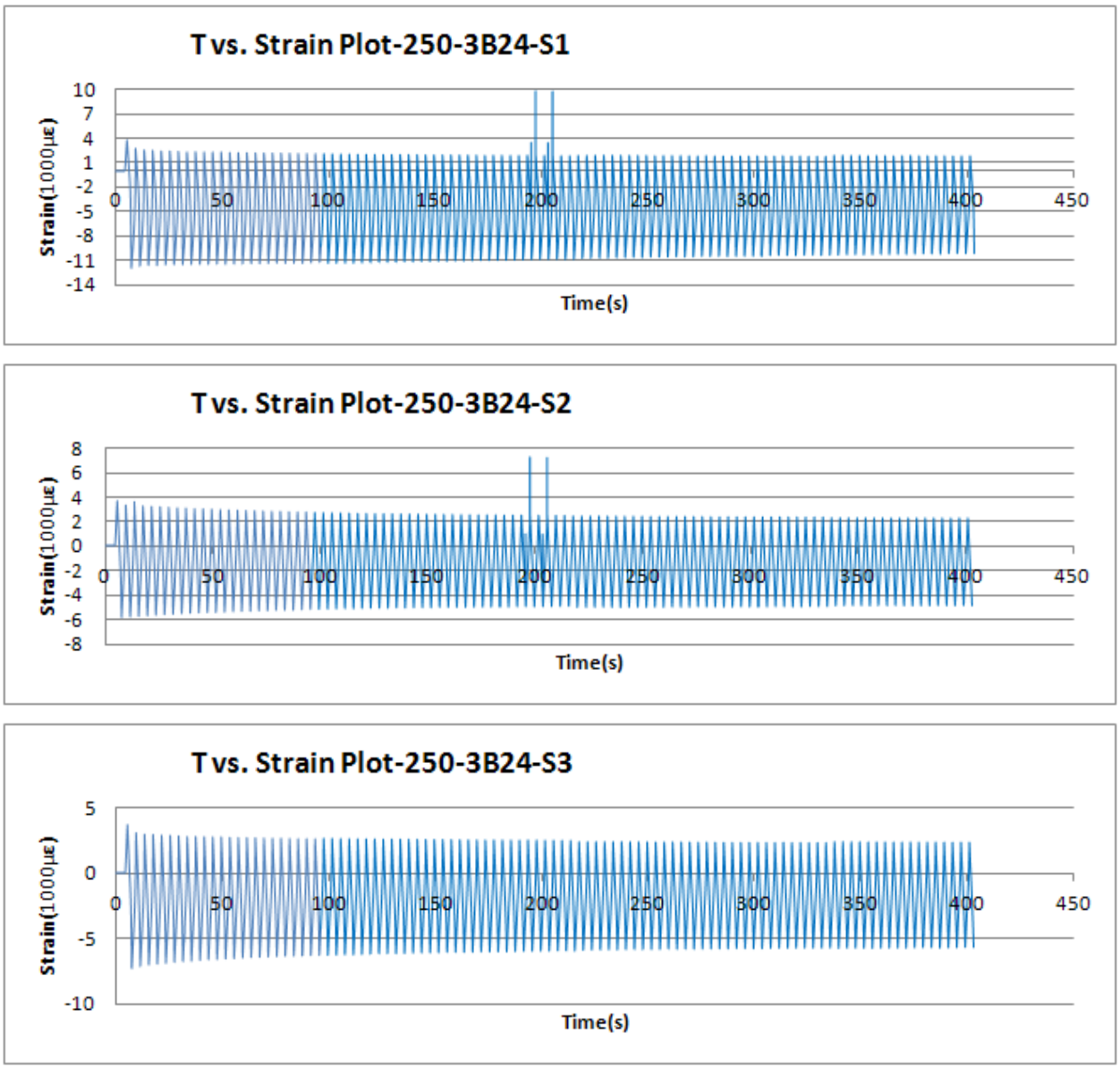


**Figure** 11(a) Time vs. Strain curve plots of $S_1$, $S_2$ & S3at 250 MPa stress for sample 3B24

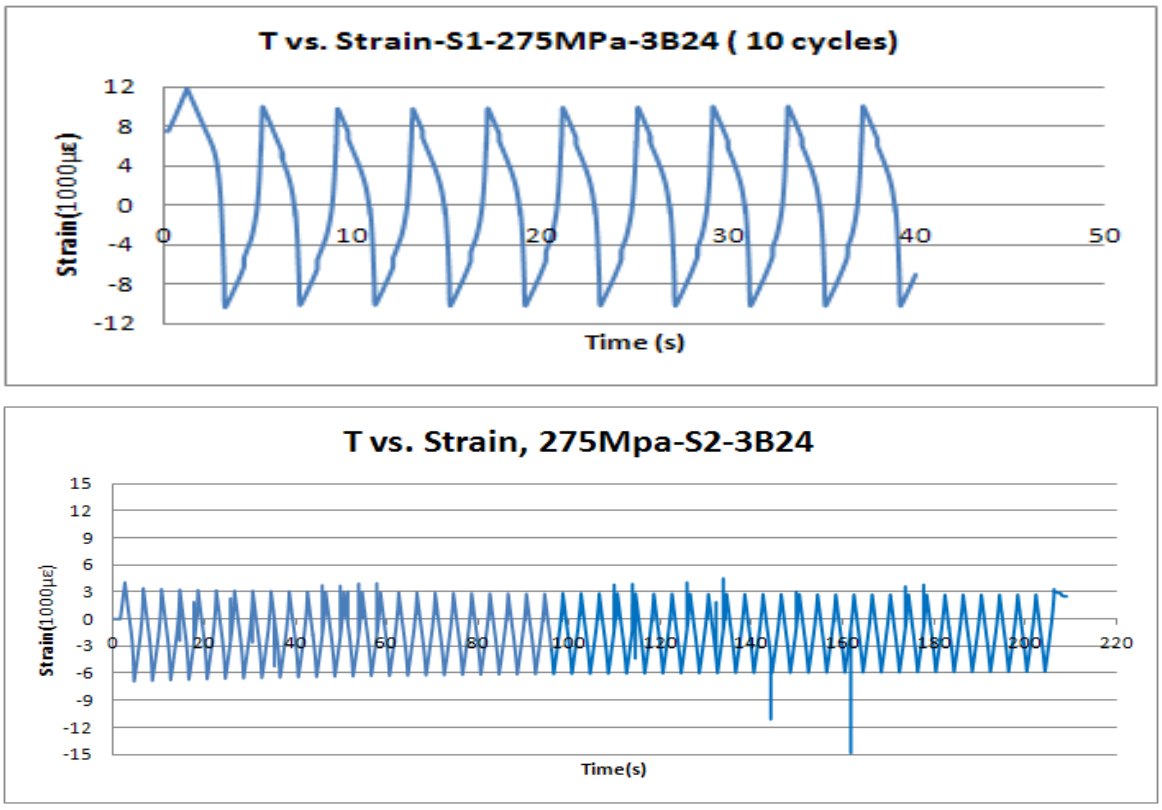


Figure 11(b), Time vs. Strain curve of $S_1$ and $S_2$ at 275 MPa stress of sample 3B24

5.4.2 **Sample 2T25.** Strain curve as a function of time for three sensors as shown below:

275 MPa stress level was applied. Sensor 3 could not sustain further to interrogate the test characteristics, figure 11(c).The reason for breaking Sensor 3 could be the bonding issue as this was located at the edge but sensor 1 and sensor 2 sustained the stress. The time vs. strain curve shows that the sample material became harder with time. Figure 11 (d) showed that with the increase stress level at 300 MPa, sensor2 sustained up to the crack point and it happened at 34$^{th}$ cycle. AT the beginning of 275 MPa $S_2$ Strain amplitude is almost ±5500με and after 90$^{th}$ cycle it has reduced to ±4000με. And at 300 MPa the starting strain was about ±5000μ€ and ended with about ±4500με, which shows that with the increasing of fatigue cycles strain amplitude reduced.

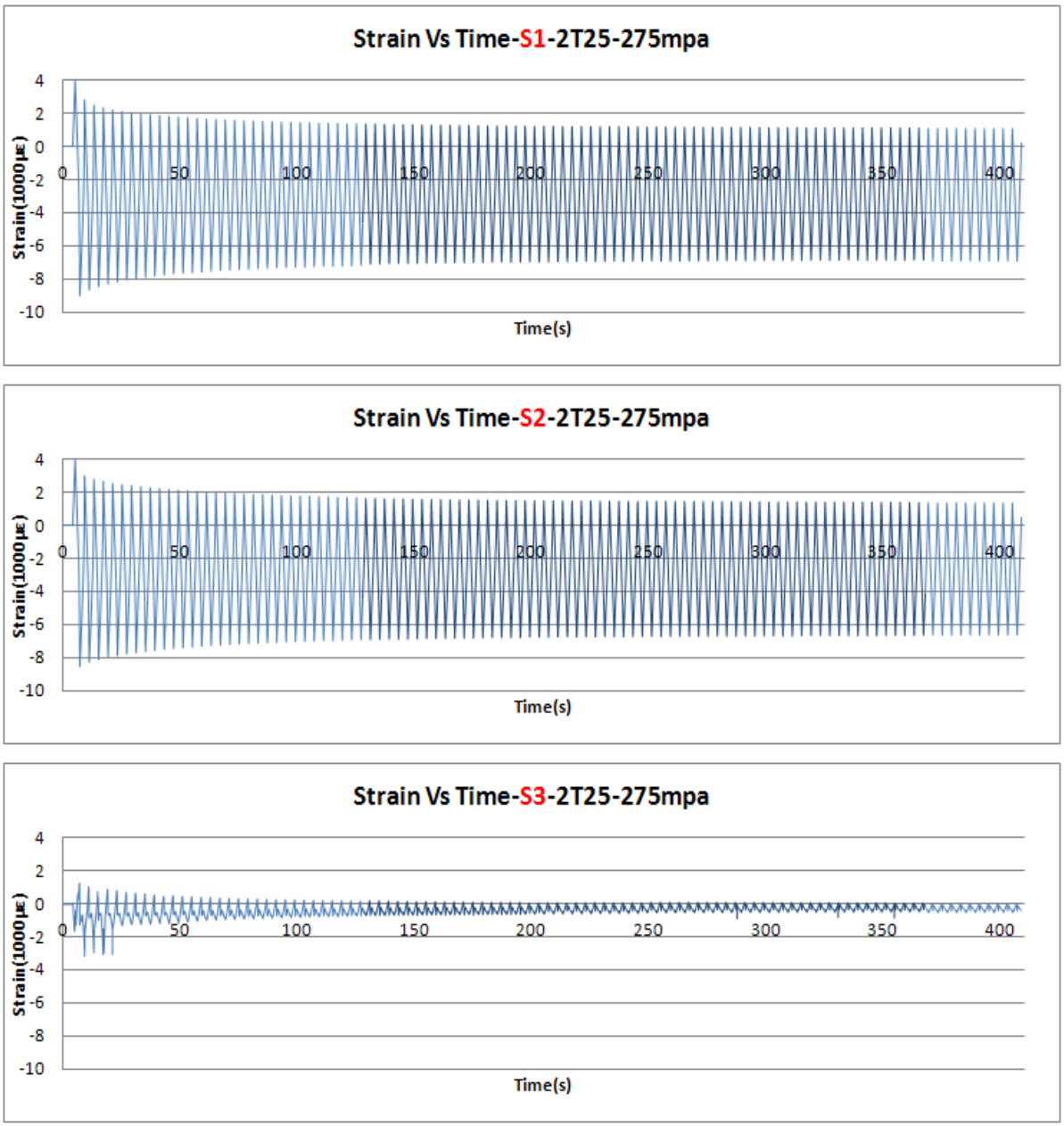


Figure 11(c), Time vs. Strain curve of $S_1$, $S_2$ and $S_3$ at 275 MPa of sample 2T25

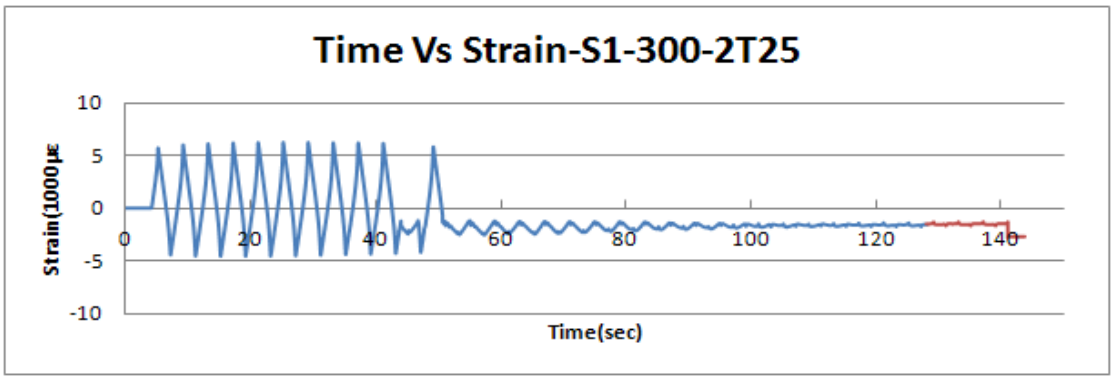


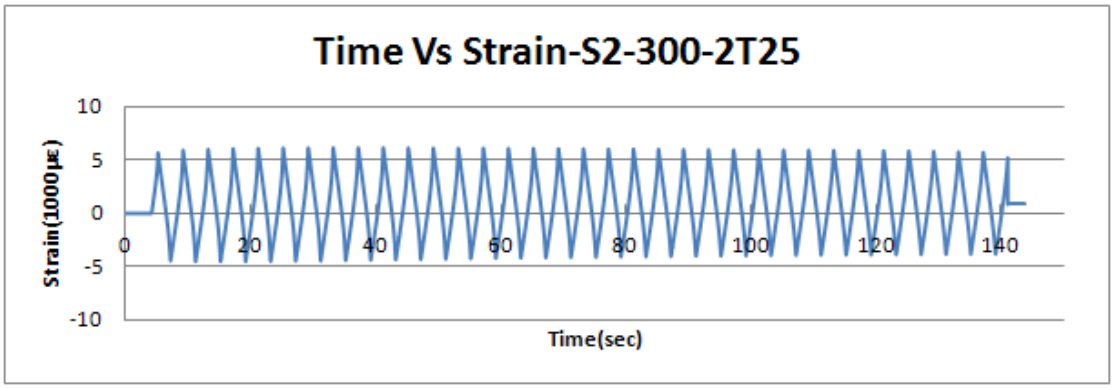


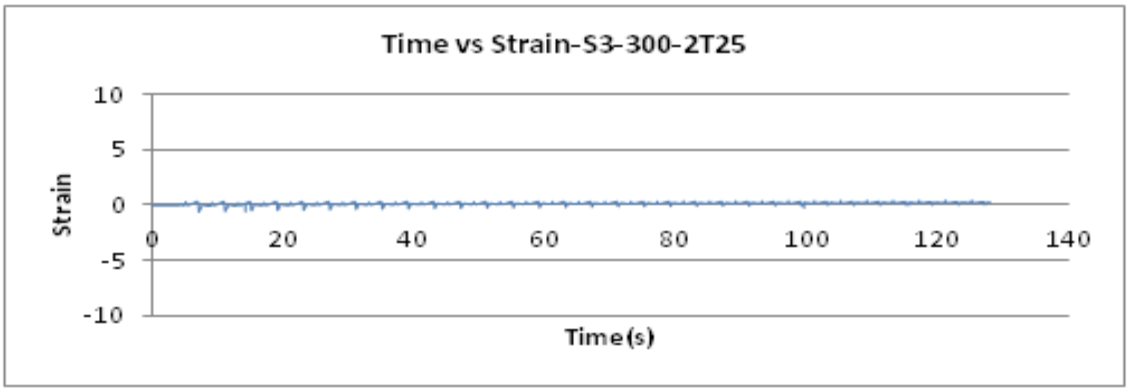


Figure 11(d), Time vs. strain curve of $S_1$, $S_2$ & $S_3$ at 300 MPa of sample 2T25

## 5.5 **Cyclic Stress and Strain Behavior**:

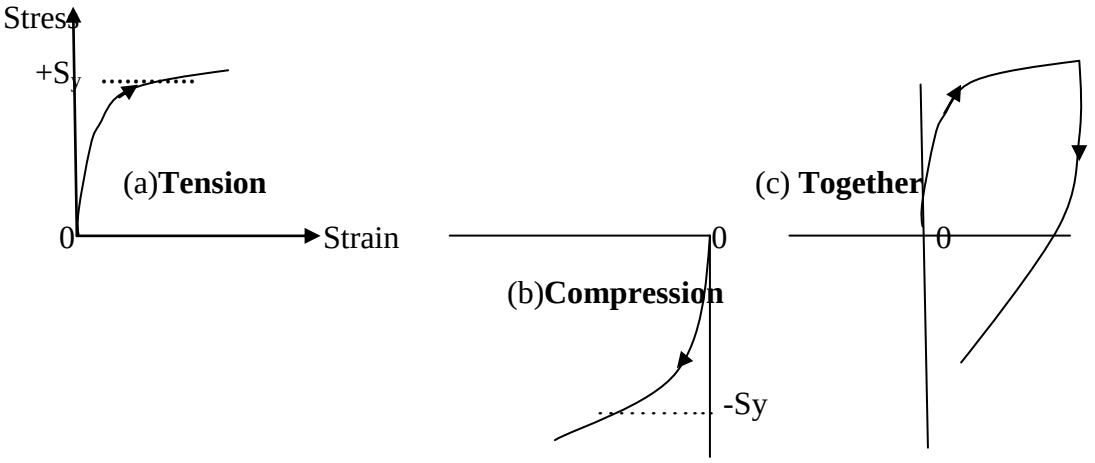


Figure 12(a), Tension loading 12(b), Compression Loading 12(c) Tension Loading followed by compression.

According to Smith et al [31] at frequencies of less than 1000 cpm the fatigue strength generally decreases with a decrease in cyclic rate. They recommended the use of a cyclic rate of between 50 and 100 cpm for low-cycle fatigue tests to (a) avoid the generation of excessive heat in the specimens, (b) keep test' time within a reasonable length, and (c) reduce to a minimum the speed effect. According to H**.** Zyad [32] the basic stress-strain curve characterizes of plastic stress-strain response of the material for the major part of the fatigue life, and is one of its most important fatigue characteristics. The strain hardening exponent (*n*) and the strength coefficient (*k*) were determined by plotting the stable stress amplitude against the axial plastic strain amplitude on a logarithmic scale for both alloys are superimposed for comparison, which shows that the value of (n) and (k) of the alloy AA7020-T6 more than of the alloy AA2024-T6. This means the high movement dislocation that produced from internal strain about precipitation atoms was occurred, and provided more grain boundaries to prevent crack propagation than in alloy AA2024-T6.

5.5.1 **250 MPa of Sample 3B24:** Hysteresis curves of LCF test for three FBG sensors are plotted as shown below:

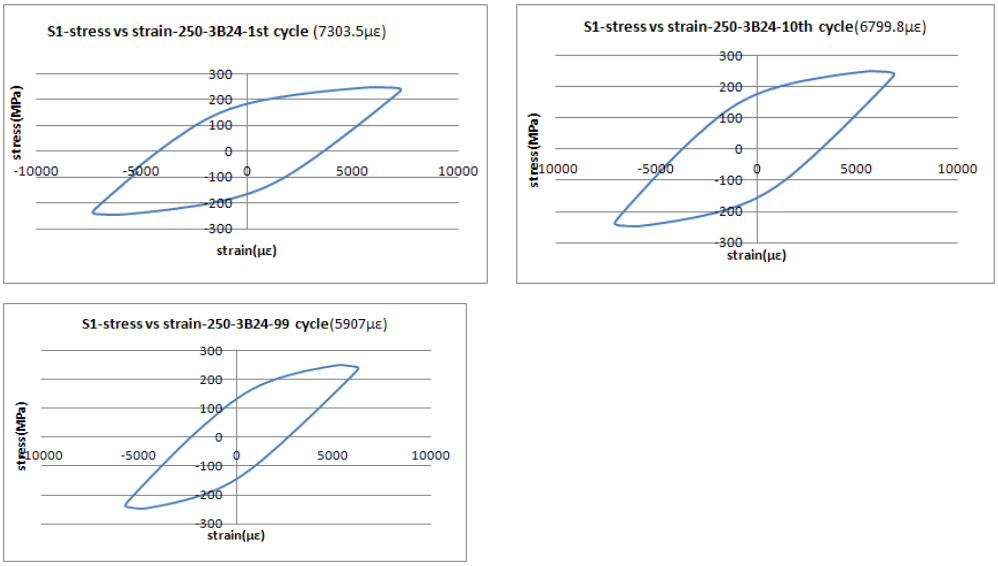


Figure 13(a), Stress vs. strain of S1 at 250 MPa of sample 3B24

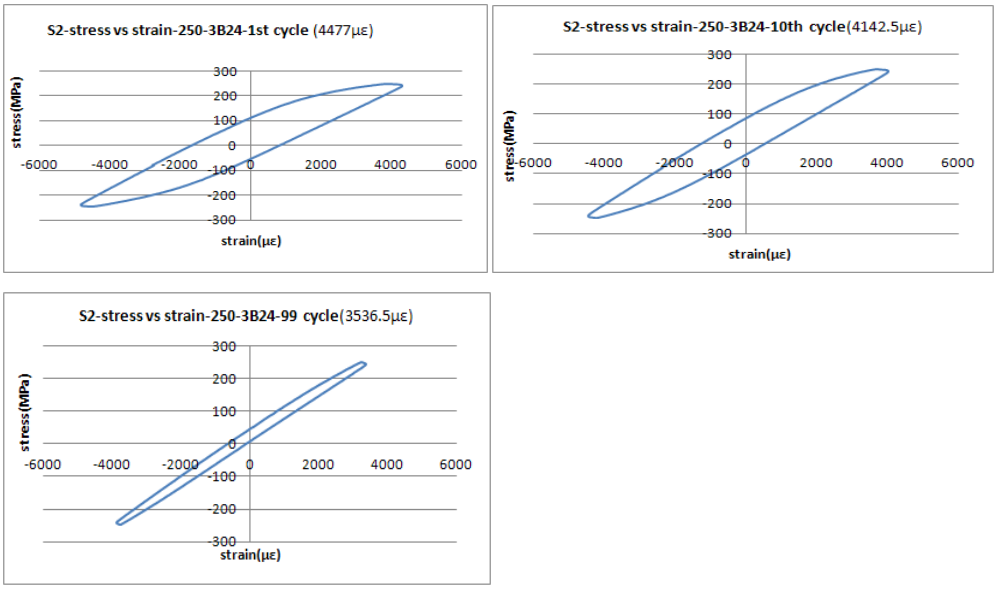


Figure 8(b), Stress vs. strain curve of $S_2$ at 250 MPa of sample 3B24

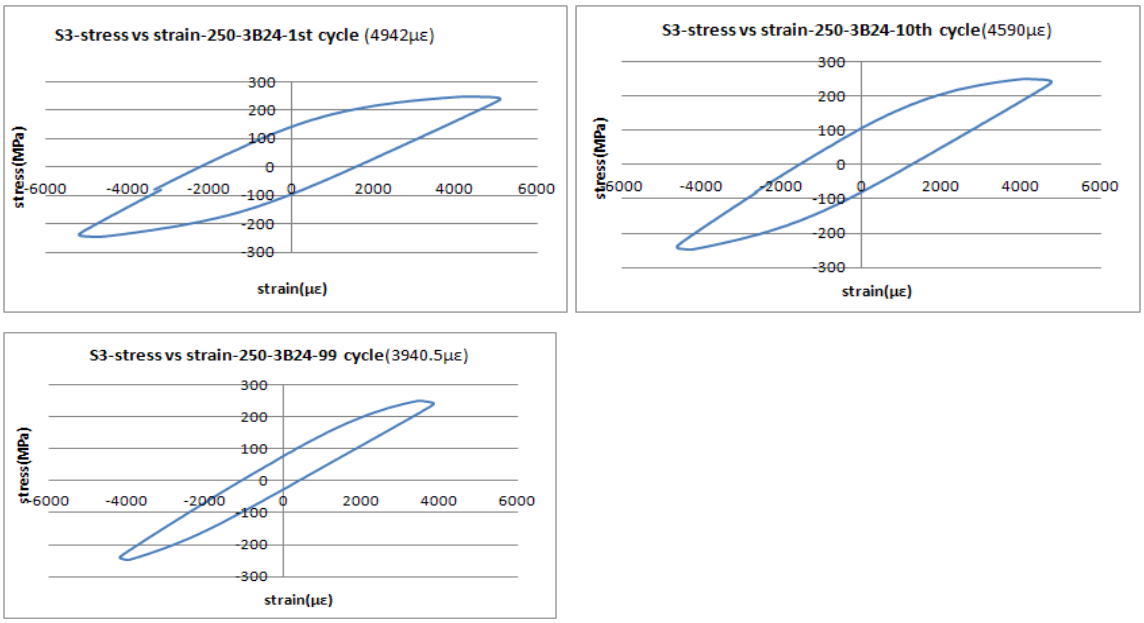


Figure 13(c), stress vs. strain curve of $S_3$ at 250 MPa of sample 3B24

5.5.2 **275 MPa of Sample 3B24:** Hysteresis curves of LCF test for S1 and S2 are plotted as shown below:

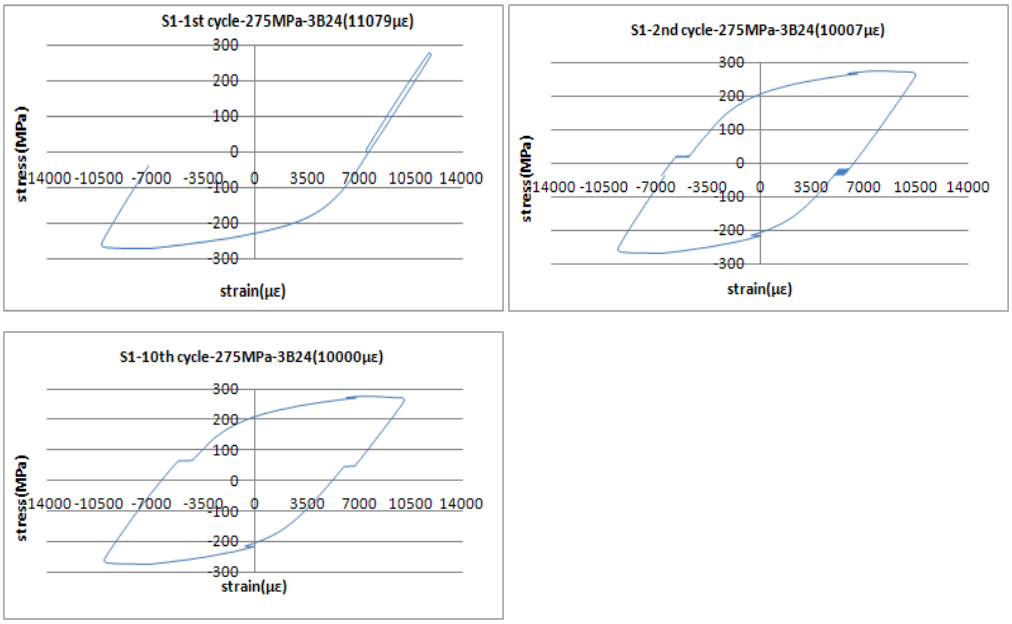


Figure 13(d), stress vs. strain curve of S1 at 275 MPa of sample 3B24

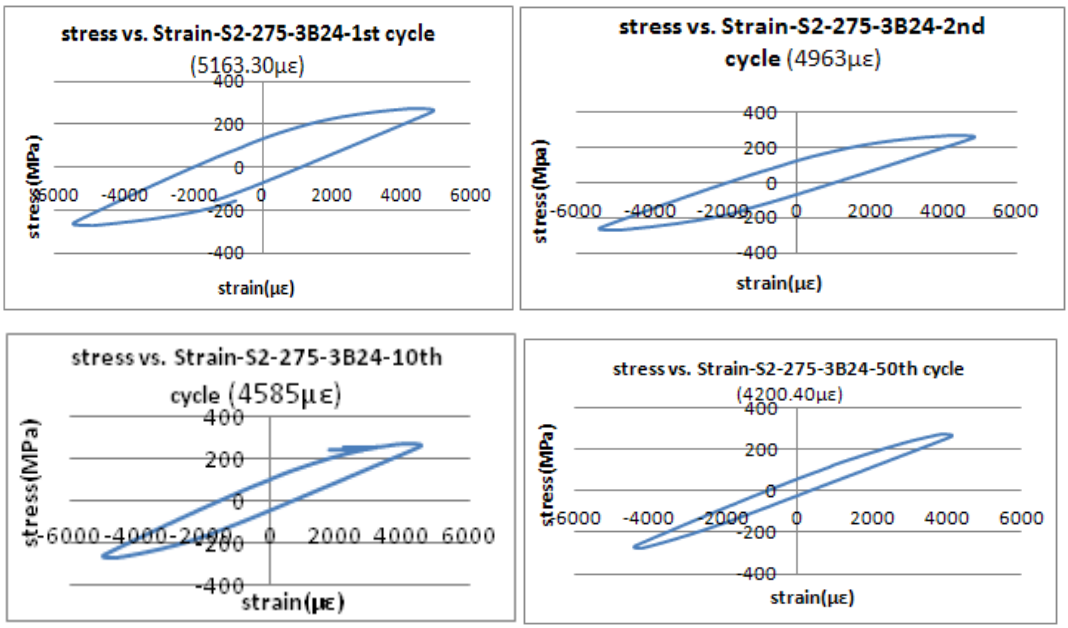


Figure 13(e), Stress Vs. strain curve of $S_2$ at 275 MPa of sample 3B24

**For sample 3B24**, in figure 13(a) to 13(c), sensor 1 and sensor 3 at 250 MPa stress were less hardening in comparison with 275 MPa, where strain amplitude (1st cycle 7303με to100th cycle 5907με and 4942με to 3940με respectively) indicate that in heated zone (HZ) the material projected less hardening than nugget zone (NZ) at the center. Whereas, in figure 13(b) for sensor 2, the hardening is more pronounced as it is the NZ which is much stronger than the HZ and thermo mechanical affected zone (TMAZ). Figure 13(d), at 275 MPa stress sensor1 sustained up to 10th cycle and figure 13(e) sensor 2 did continue till the end and I observed steady hardening of the Al alloy with the time.

5.5.3 **275 MPa- Sample 2T25:** Hysteresis curves of LCF test for S1 and S2 are plotted as shown below:

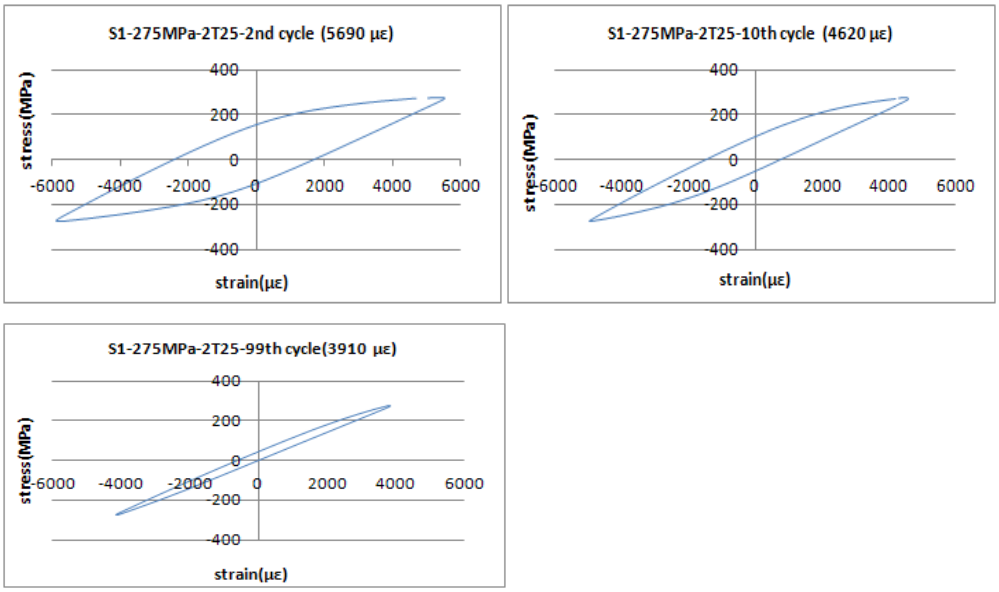


Figure 13(f), stress vs. strain curve of $S_1$ at 275 MPa of sample 2T25

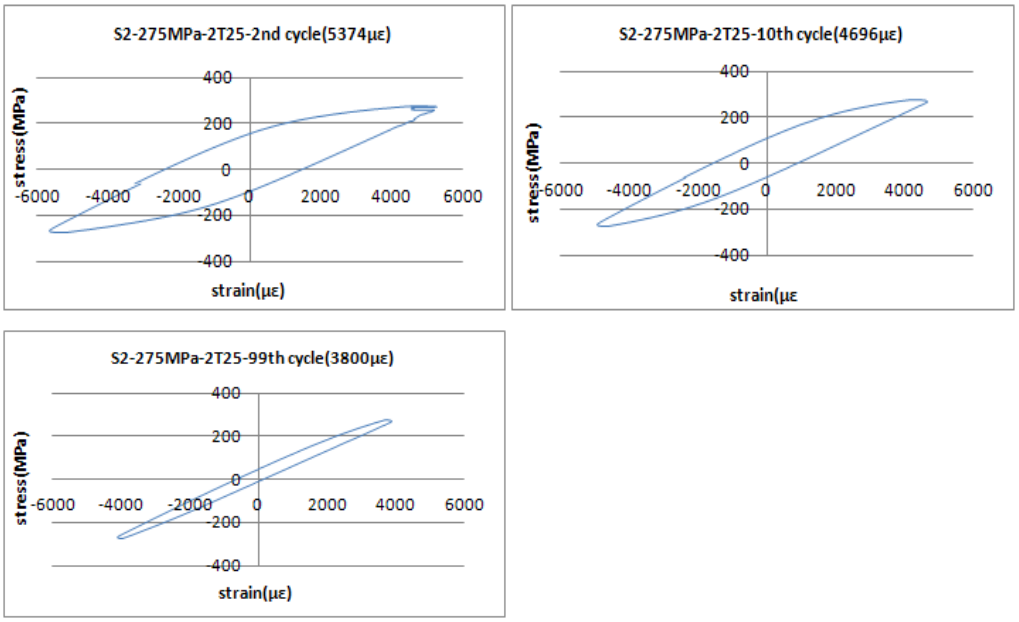


Figure 13(g), Stress vs. strain curve of $S_2$ at 275 MPa of sample 2T25

5.5.4 **300 MPa-Sample 2T25:** Hysteresis curves of LCF test for S1 and S2 are plotted as shown below:

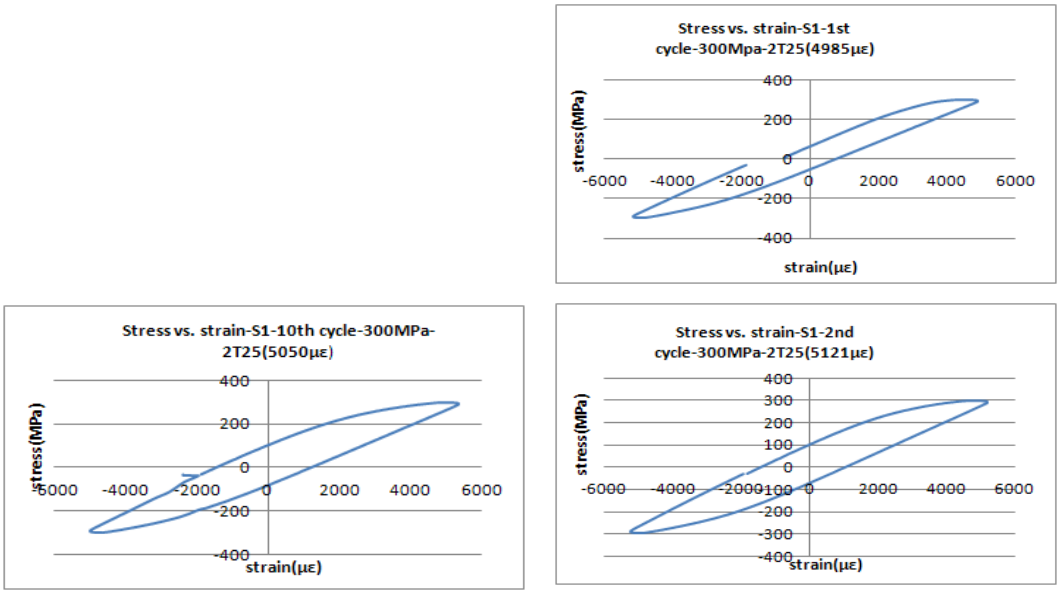


Figure 13(h), stress vs. strain curve of $S_1$ at 300 MPa of sample 2T25

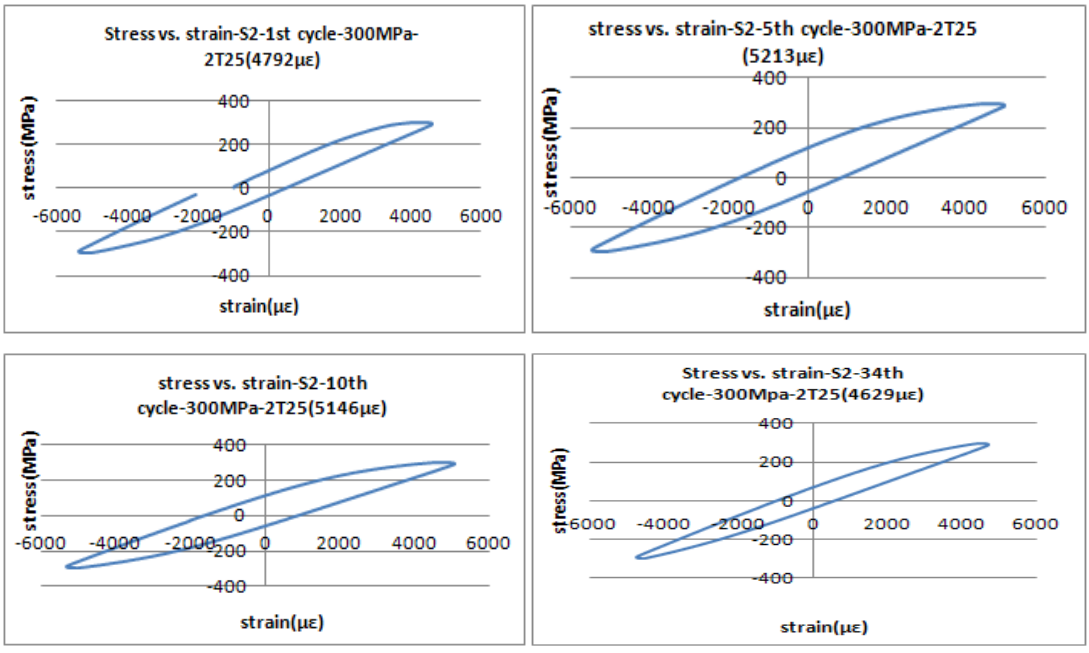


Figure 13(i), stress vs. strain curve of S2 at 300 MPa of sample 2T25

**For sample 2T25**, at 275 MPa stress level the deformation was observed quite large and sensor 3 failed to respond and the reason for failing could be the bonding issue as it was located at the edge of the gauge area. Sensor1 and sensor2 both shows steady hardening characteristics with cycle as shown in figure 13(f), 13(g) where the strain ranges ($1^{st}$ cycle 5705με to $100^{th}$ cycle3965 με for S1 and 5342με to 3965με for S2) respectively. Sensor1 with the shortest wavelength was located closer to blue mark and at this point S1 was subjected to maximum stress which caused it to break. Another reason could be the bonding issue as it was located at the edge of the gauge area. But S2, as shown in figure 13(i), responded till last cycle of sample failure. In both the case I observed the same deformation characteristics.

The strain range for each sensor and cycle are different due to the following factors:

(a) At different locations the material characters of the sample are different. This in turn results the difference in strain amplitude.

(b) As the fatigue life of the material is inversely proportional to strain, with the increase in cycles the strain of the sensors decreases. In our experiment mostly decrease was observed.

### 5.6 **Plastic strain amplitude (PSA) analysis:**

The cyclic deformation response is expected to be influenced by the applied cyclic stress or strain, more importantly by the cyclic plastic strain. Such influence from the applied cyclic plastic strain is evidence from the observed transition from cyclic hardening to cyclic softening with increasing applied cyclic plastic strain [13].

#### 5.6.1 Behavior Analysis of material from PSA curve:

In LCF, PSA is a physical quantity that initiates several damaging process and influences the internal microstructure which eventually affects the strain resistance and finally the fatigue life. The cyclic deformation response of metal ranging from cyclic hardening to cyclic softening depends on various factors like the purity of the metal, the level of the imposed cyclic stress/strain, and the processing parameters [13]. In figure 14(a, b, c, d) of the test results it was observed that when total strain amplitude increases PSA also increases and fatigue life decreases. During initial few cycles the curves change was steep, after initial few cycles the slope becomes

steady with the increase of the number of cycles. In both samples of 3B24 and 2T25 the gradual cyclic hardening of the material and gradual decreases of sensors PSA was observed.

**For sample number 3B24** at 250 MPa stress level in figure 14(a) PSA range of sensor 1 (0.04% to .025%) had steadily reduced, indicating gradual hardening. The PSA range of sensor2 (0.15% to 0.002%) showed the same behavior like sensor1.PSA range of sensor 3 (.022% to .0053%) showing similar hardening. In figure 14(b) at 275 MPa stress level, for sensor 2 the PSA (0.018 to 0.0051%) showed the significant hardening of the material up to the crack which occurred at 50$^{th}$ cycle. However, S1 and S3 failed at this level, initial two cycles were very sharp and they became steady with fatigue cycles.

5.6.2 Study of Plastic Strain vs. Cycles at different stress levels (Each sensor separately).

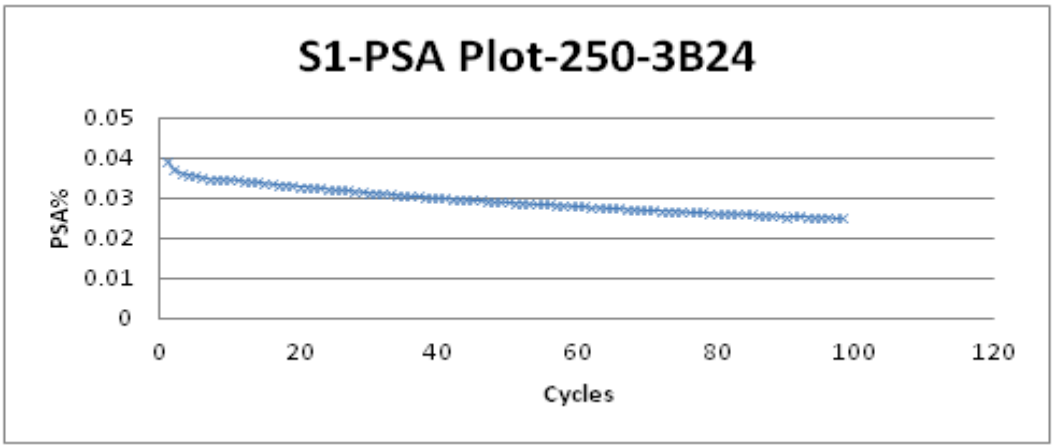


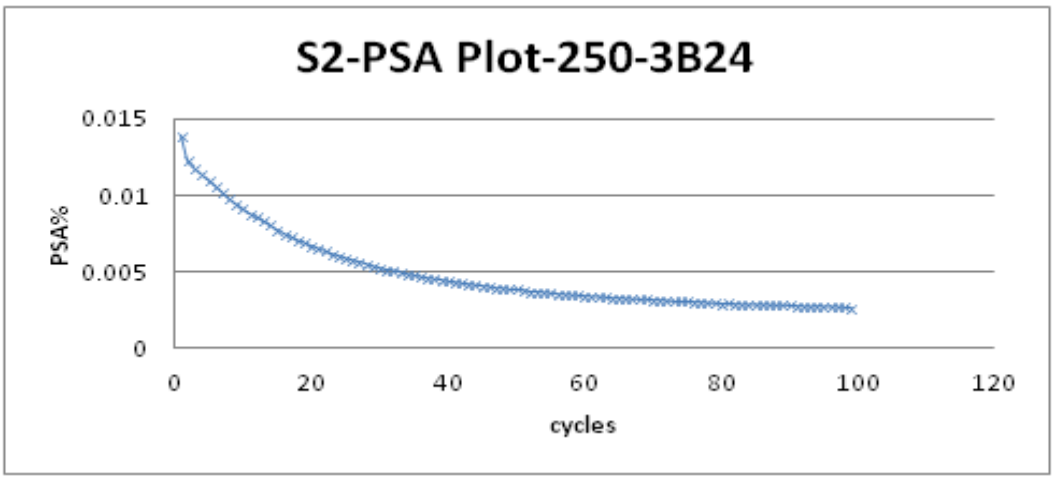

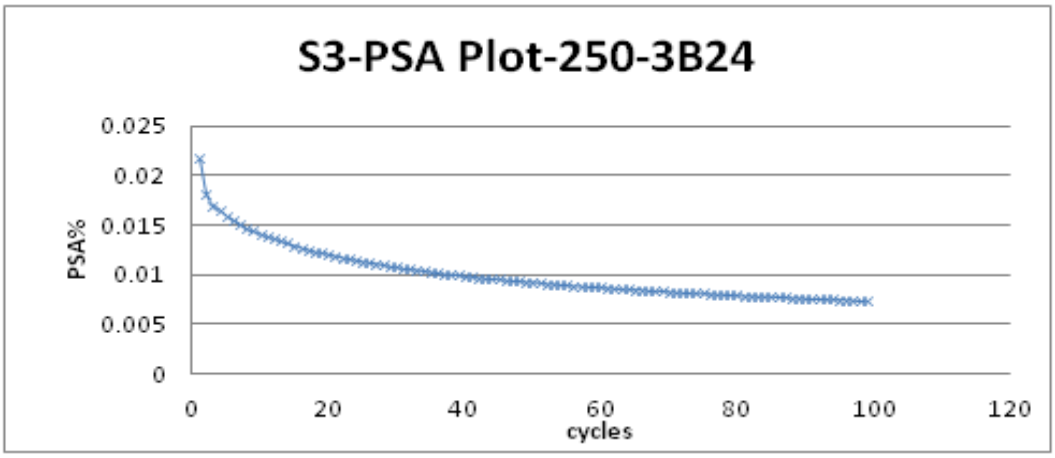


Figure 14(a), PSA vs. cycles curve of S1,S2 & S3 at 250 MPa of sample 3B24

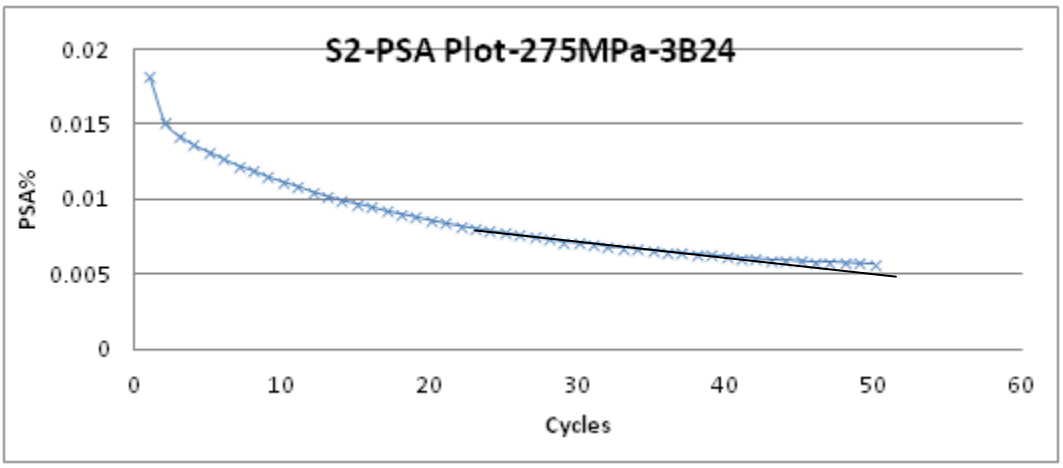


Figure 14(b), PSA vs. Cycles of S2 at 275 MPa of sample 3B24

5.6.3 Comparing the difference of response of Sensor2 between 250 MPa and 275 MPa with PSA as a function of cycles (Sample 3B24):

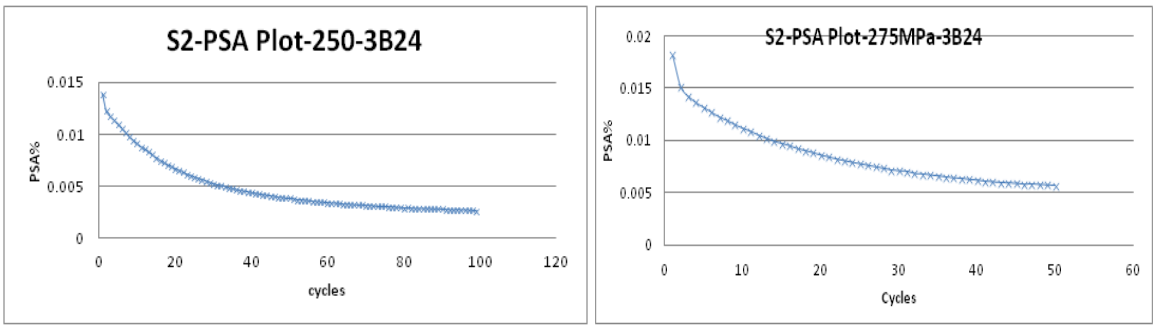


Figure 14(c) and 9(d) PSa of 3B24 at 250 MPa & 300 MPa

(i) Figure 14 (c) showed the deformation of the sample at 250 MPa was less than at 275 MPa in which from 1st cycle to 30th cycle PSA% reduces (.014% to .005%) , whereas, in figure 14(d)

at 275 MPa it reduces the PSA%(.02% to .01%) showing more deformation and more hardening.

(ii) Again, from 31st cycle till last at 250MPa it reduces the PSA% (.006% to .0025%).On the other hand, at 275 MPa the changes are .01% to .0051%, which showed more hardening and deformation of the FSW.

5.6.4 **For sample 2T25** at 275 MPa stress level figure 14(e), both sensor 1 and sensor2 are showing almost identical PSA change which ranging (0.014 % to 0.002% and 0.15% to 0.002%). The hardening is also gradual and significant. At 300 MPa level, sensor 1 could monitor only up to 10th cycle and more observations could not be obtained but sensor2 could respond up to the crack point (34th cycle). I can notice from figure 14(g), that the PSA from 0.13% to .008% was significant hardening of the material. Here also I observed the same behavior like other samples of softening with initial few cycles.

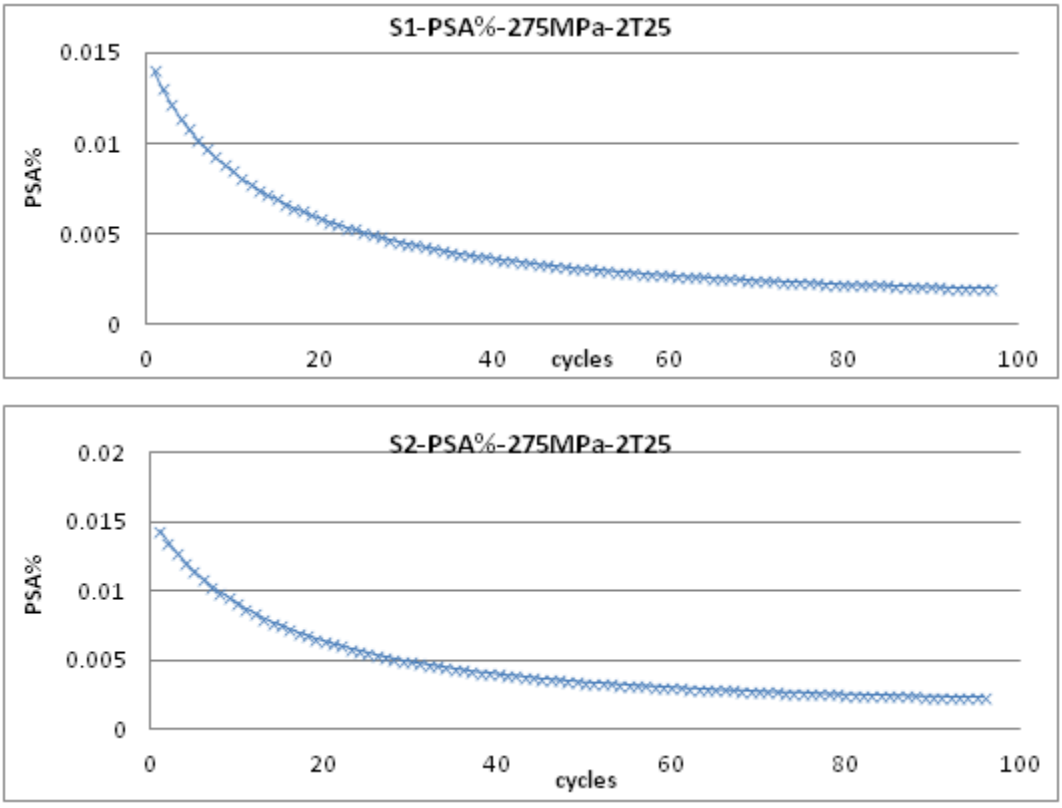


Figure 14(e), PSA vs. cycles of S1 & S2 at 275 MPa of sample 2T25

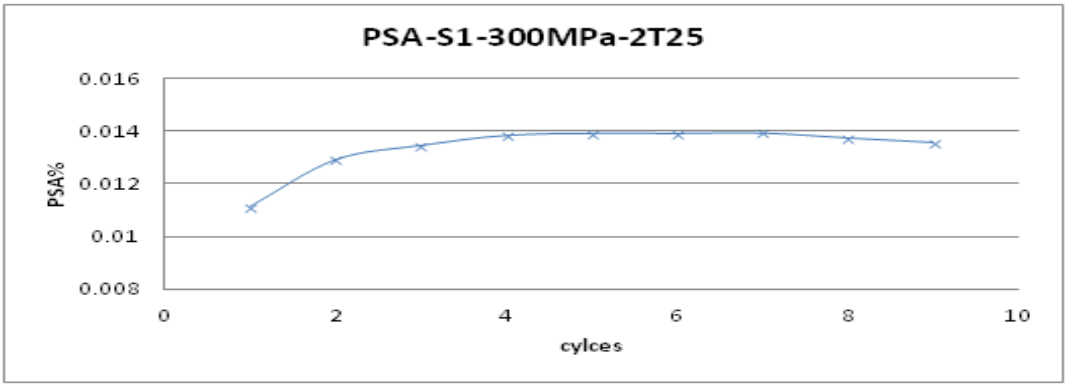


Figure 14(f) PSA% of S1as a function of cycles

At 300 MPa level sensor 1 could monitor only up to 10$^{th}$ cycle and more observations could not be obtained. But sensor2 could respond up to the crack point (34$^{th}$ cycle) and noticed from figure 14(g) that the PSA% (0.13% to .008%) which is significant hardening of the material. Here also it is observed the same behavior like other samples of softening with initial few cycles.

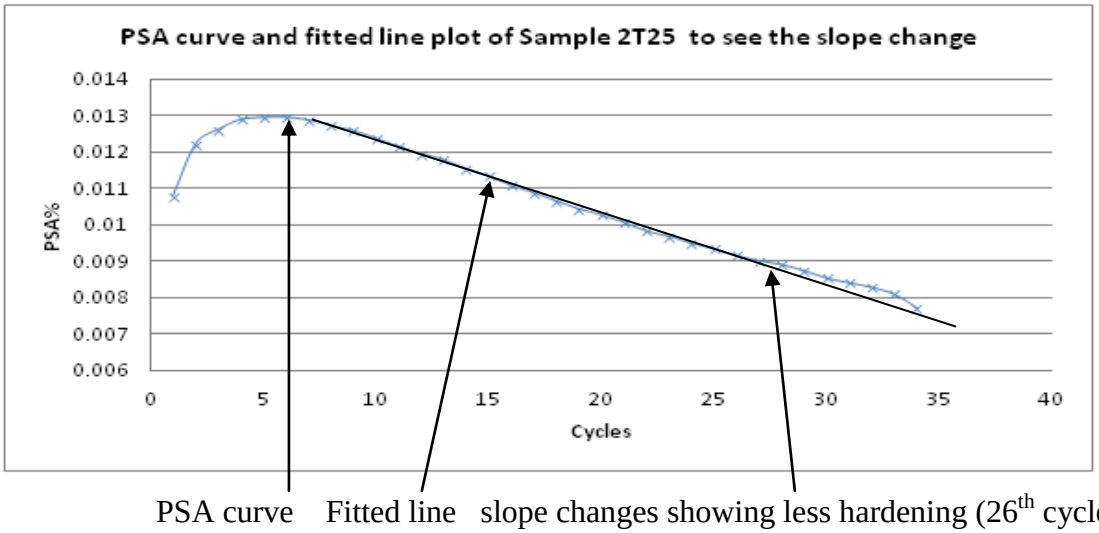


PSA curve Fitted line slope changes showing less hardening (26$^{th}$ cycle)

Figure 14(g), PSA curve and linear fit from cycle 7 to 21

The PSA curve plotted at 275 MPa for sample 2T25 [figure 14(g)] showed the following characteristics:

(i) In initial five cycles the PSA increased from .0108% to .013% and material Showed softening characteristic which could be interpreted as crack initiation.

(ii) From the 6th cycle till 25th cycle the PSA value was reducing almost linearly (from .0129% to .0091%), indicating cyclic hardening characteristics as shown in the fitted line in figure 14(g) and this could indicate crack propagation .

(iii) After 25th cycle the PSA slope started to deviate significantly from the previous 20 cycles as shown in figure 14(g). This sudden changed (less hardening) in slope could be an indication of the severe crack growth which led to ultimate failure of the sample, occurred at 34th cycle.

5.6.5 Difference in response of Sensor2 from PSA curve at 275MPa & 300 MPa (2T25)

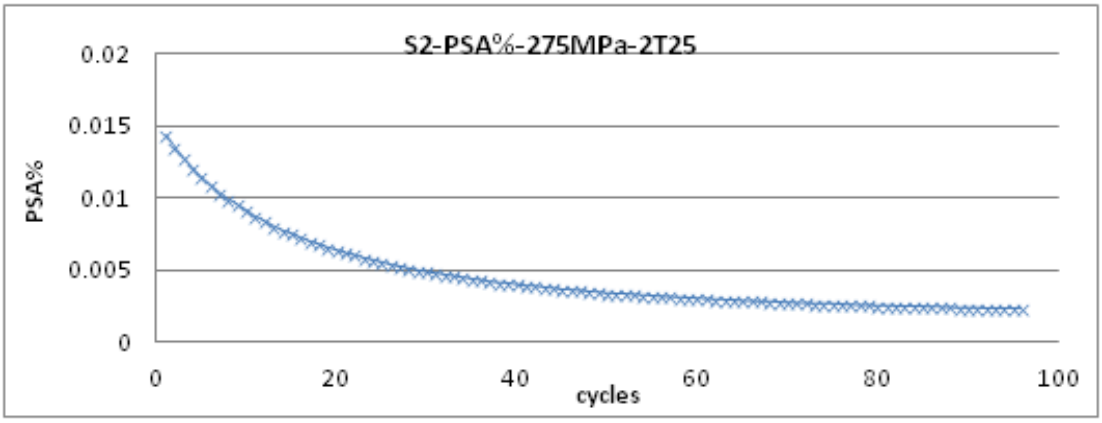


Figure 14(h) PSA at 275 MPa

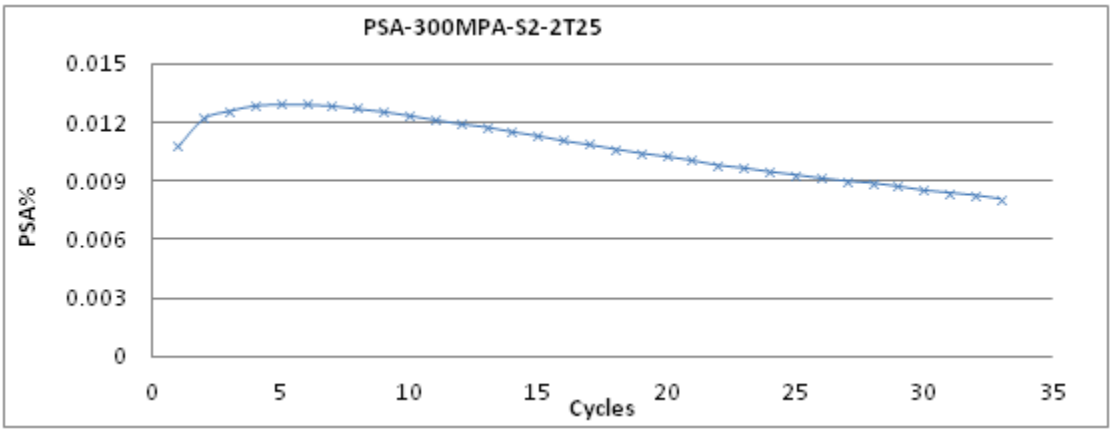


Figure 14 (i) PSA at 300 MPa of 2T25

It is worthwhile to compare the PSA curves at two different stress levels, 275 MPa and 300 MPa:

(i) In figure 14 (h) the PSA slope change monotonically, whereas, at 300 MPa PSA curve can be divided in three sections namely (1st cycle – 6th cycle), (7th cycle – 25th cycle) and (26th cycle – 34th cycle) respectively.

(ii) In figure 14 (h) the curve shows cyclic hardening monotonically with no sudden variation in the slope .However, in figure 14(i) major changes of PSA slope were observed in three sections in term of its PSA amplitude values and direction.

## 5.7 **The Sample Response of Strain Amplitude as function of cycles:**

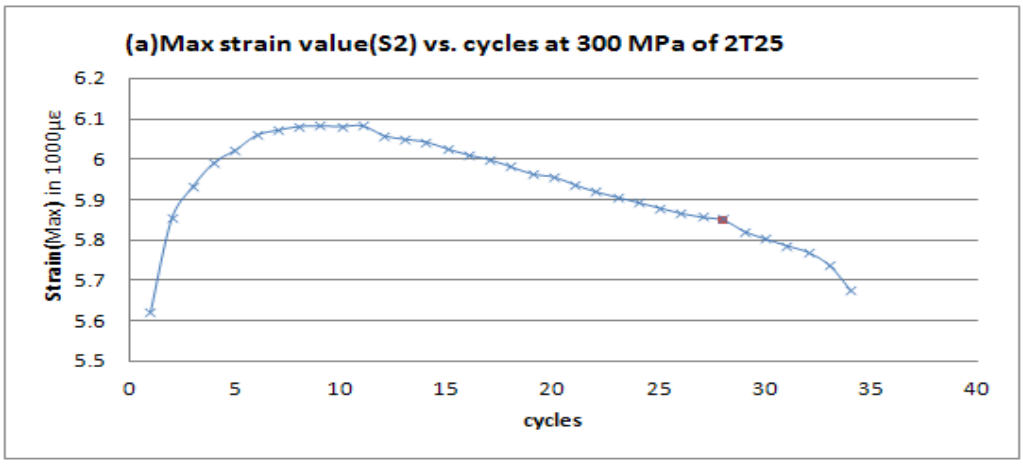


Figure 15 (a), Maximum tensile strain ($\varepsilon_{max}$) response as a function of Cycles

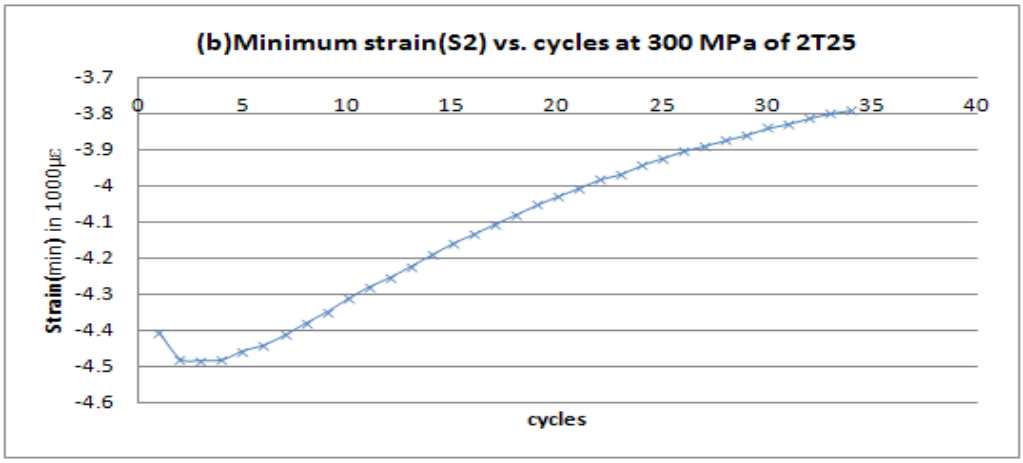


Figure 15 (b), Minimum Strain ($\varepsilon_{min}$) response as a function of Cycles

As we know, maximum strain and minimum strain is opposite and from the above figure 15(a) and 15(b) it is observed that their response as a function of cyclic load is also opposite. Figure 15(a) region-I, confirms the softening of the metal with increase in strain amplitude whereas, figure 15(b) initially it is decreasing with reduced strain value.

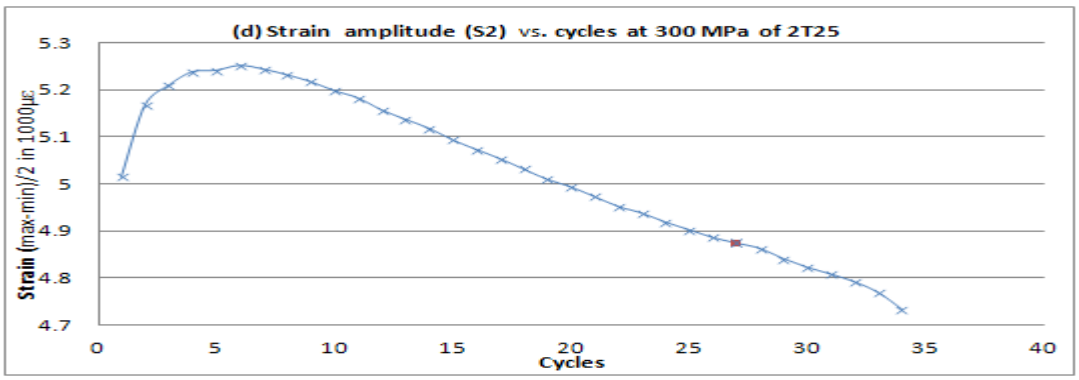


Figure 15(c), Strain amplitude [$\varepsilon_a = (\varepsilon_{max} - \varepsilon_{min})/2$] as a function of cycles

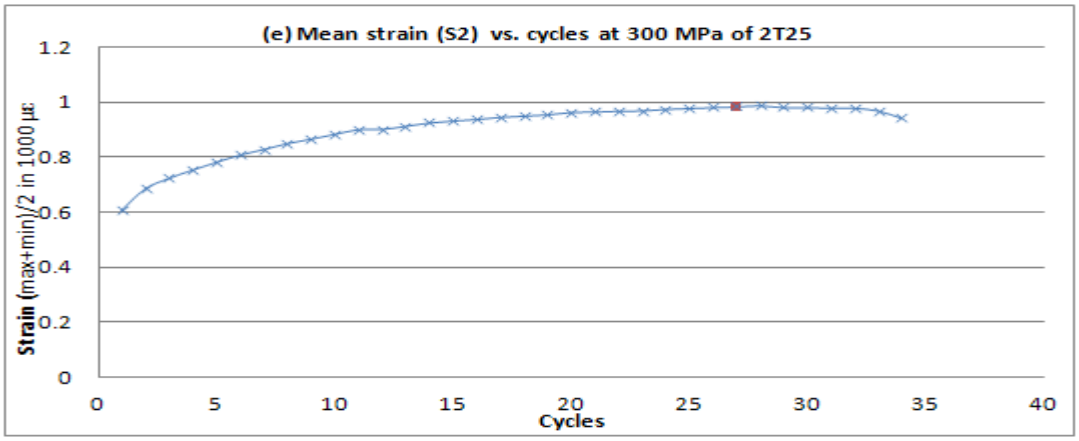


Figure 15 (d), Mean strain [$\varepsilon_m = (\varepsilon_{max}+\varepsilon_{min})/2$] as a function of cycle

From figure 15(a) and 15(c), by plotting strain range and strain amplitude as a function of cycles, we observe the followings:

- There are also three regions in the curves.
- From 1st cycle to 6th cycle strain amplitude is increasing (showing softening), from 7th cycle to 25th cycle changes direction and reducing almost linearly (showing hardening). Again from 26th cycle to 34th cycle, the slope of strain amplitude reduction happens, though less visible than that in figure 14(g). The variation of strain amplitude, changing direction and changing slope corresponds well with the PSA variation.

5.7.1. Comparing the minimum and maximum strain amplitude curve, the following points are also observed:

- During maximum strain figure 15(a) the change in the curve at three sections are the evidence of deformation and as it reduced its value up to maximum cycle which indicated its hardening characteristic with cycles progress. And with changing its curve upward after $26^{th}$ cycle showed less hardening which was the indication of ultimate macro crack.
- On the other hand, with minimum strain, figure 15(b) the curve is almost linear, which indicates that it is not as indicative to illustrate sample deformation.

## Chapter 5

# 6. Conclusion and Future Work

## 6.1 **Conclusion**:

The intention of this research was to use FBG sensors to detect the crack initiation of aluminum alloy. The small size and light weight allow the FBG to detect localized strain. The experiments data proved that FBG sensors could be used to detect the crack initiation and to characterize the response of metal with increased applied stresses. The large contact area of the FBGs made on flat cladding fiber, together with an enhanced bonding process, has significantly increased strain measurement range. From the analyses of the data, following concluding points can be highlighted:

(i) The flat cladding FBG sensors are used to measure the cyclic strain amplitude up to ± 11000με ( figure, 13(d)] for aluminum fatigue test.

(ii) Cyclic hardening was observed as demonstrated by the PSA decreasing with the cycles number. Significant change in PSA slope was observed at ~8 cycles before the fatigue failure happens which was interpreted as the crack propagation.

(iii) Although fatigue failure occurred in TMAZ zone, the significant deformation also occurred in NZ. FBG measurements showed that it is possible to detect the failure several cycles before it occurs.

## 6.2 **Suggested Future Work**:

The crack initiation and material failure detection could be better resolved by sensors during the test stages of LCF testing system provided that the sensors are able to sustain up to higher stress level. Especially, the sensors are at edges may be given more attention during bonding. To increase the bonding strength, the use of weight during cure should be more balanced so that the sensors at the edges may overcome the weaknesses, which is observed during these tests. Also the multiplexed FBG sensor array could be applied to measure strain distribution in mechanical and material components, as well as for structural health monitoring. To view the fracture surface and propagation region Scanning Electron Microscope (SEM) micrographs may be used to verify the analyzed result.

**References:**


[1] C. Li, A. Feng, X. Gu, and D.Chen, "Localized Cyclic Strain Measurements of Friction Stir Welded Aluminum Alloy Using a Flat Clad Optical Fiber Sensor Array", IEEE Sensors Journal, Vol.10.4, pp.888-892 April 2010.

[2] M. Bass and E. Stryland: Fiber Optic Handbook: Fiber, Devices, and Systems for Optical Communication, OSa, Mcgraw-Hill, 2002.

[3] H. Lu, R. Hussain, M. Zhou and X. Gu, "Fiber Bragg Grating sensors for Failure Detection of Flip Chip Ball Grid array in Four-Point Bend Test", IEEE sensors Journal, vol.9(4), pp.457-463,2009.

[4] J. Yao and W. Munse, " Low-Cycle Fatigue of Metals" , Ship Structure Committee, U.S Coast guard Headquarters, Washington 25, D.C, October 31, 1961.

[5] G. Bahareh and N. Hooman, "Fiber Optic Sensors", World Academy of Science, Engineering and Technology 42 2008.

[6] M. Patrice, B. Sebatien, C. Cathy and C. Christophe, "Fiber Bragg Gratings: fundamentals and applications", 3rd May 2007.

[7] B. Culshaw, J. Dakin, "Optical Fiber Sensors", Boston, Artech House, c1988-c1997.

[8] Yu, S. Yin, "Fibre optic sensors", Marcel-Dekker, 2002.

[9] K. Delong, C. Jun, and et al, "Analysis and Improvement of SNR in FBG Sensing System", School of Information Science and Engineering and Shandong Provincial Key Laboratory of Laser Technology and Application, Shandong University, Jinan, 250100, China, Photonic Sensors (2012) Vol. 2, No. 2: pp.148–157.

[10] N. Isa and A. Ahmet, "Design of a Chirped Fiber Bragg Grating for use in Wideband Dispersion Compensation", www.emo.org.tr/ekler/0b45d1bb84fe1be_ek.pdf.

[11] ASM International, "Elements of Metallurgy and Engineering Alloys- Fatigue", (#05224G), 2008. www.asminternational.org.

[12] R. W. Smith, M. H. Hirschberg, and S. S. Manson, "Fatigue Behavior of Materials under Strain Cycling in Low and Intermediate Life Range", NASA, TN D-1574, 1963.

[13] K. Charles and W. Wang, "The Cyclic Deformation Behavior of Severe Plastic Deformation (SPD) Metals and the Influential Factors" , Department of Materials Science and Engineering, Faculty of Applied Science and Engineering, University of Toronto, Metals 2012, 2, 41-55; doi:10.3390/met2010041.

[14] Kunz, L; Lukáš, P.; Svoboda, M. Fatigue strength, micro structural stability and strain localization in ultrafine-grained copper. Mater. Sci. Eng. A 2006, 424, 97–104.

[15] Xu, C.Z.; Wang, Q.J; Zheng, M.S.; Li, J.D.; Huang, M.Q.; Jia, Q.M.; Zhu, J.W.; Kunz, L.; Buksa, M.Effect of low temperature on fatigue life and cyclic stress-strain response of ultrafine-grained copper. Mater. Sci. Eng. A 2008, p.475, pp.249–256.

[16] Kunz and et al, Stability of ultrafine-grained structure of copper under fatigue loading. Proc. Eng. 2011, 10, 201–206.

[17] Wong, M.K.; Kao, W.P.; Lui, J.T.; Chang, C.P.; Kao, P.W. Cyclic deformation of ultrafine-grained aluminum. Acta Mater. 2007, 55, 715–725.

[18] May and et al, H.W. Monotonic and cyclic deformation behavior of ultrafine-grained aluminum. Mater. Sci. Eng. A 2008, 483–484, 481–484.

[19] S. Ghiya, D. Bhatt, R. Rao, "Stress Relief Cracking in Advanced Steel Material-Overview", Proceedings of the World Congress on Engineering 2009 vol. II WCE 2009, July 1 - 3, 2009, London, U.K.

[20] S J Maddox, TWI Ltd," Review of fatigue assessment procedures for welded aluminum structures" Paper published in International Journal of Fatigue, Paper JIJF1005. vol. 25, no. 12, December 2003, pp. 1359-1378.

[21] F. Ellyin, "Fatigue Damage, Crack Growth and Life Prediction", by Springer | November 30, 1996.

[22] T. Zhao, J. Zhang and Y. Jiang, " A study of fatigue crack growth of 7075-T651 aluminum alloy" , Department of Mechanical Engineering (312), University of Nevada, Reno, NV 89557, USA, International Journal of fatigue vol. 30, Issue 7, July 2008, Pages 1169-1180.

[23] Zhi Y. Huang, W. Daniele , B. Claude , J. Chaboche, "Cumulative fatigue damage in low cycle fatigue and gigacycle fatigue for low carbon–manganese steel" , International Journal of Fatigue 33 (2011) 115–121.

[24] S.Kumar Paul, Researcher, R&D, Tata Steel Limited, Jamshedpur 831001, India, "Effect of anisotropy on ratcheting: An experimental investigation on IFHS steel sheet", Materials Science and Engineering A 538 (2012) 349– 355.

[25] Christopher Ngiau1, Daniel Kujawski, Department of Mechanical and Aeronautical Engineering, College of Engineering and Applied Sciences, Western Michigan

University, Kalamazoo, MI 49008-5065, USA, “Sequence effects of small amplitude cycles on fatigue crack initiation and propagation in 2024-T351 aluminum” , International Journal of Fatigue 23 (2001) 807–815.

[26] W. Xu, J. Liu, D. Chen, G. Luan and J. Yao, “Tensile Properties and Strain Hardening Behavior of a Friction Stir Welded AA2219 Al Alloy”, (2011) Trans Tech Publications, Switzerland, doi: 10.4028/www.scientefic.net/AMR. 291-294.833.

[27] G. Lucas, P. Mckeighan and J. Ranson, “Non Traditional Method of Sensing Stress, Strain and Damage in Materials and structures”, ASTM Stock Number: STP1323-Second Volume.

[28] C. Li, “The Fiber Optic Sensing array For Fatigue Tests”, MASC thesis, Ryerson University, September 18, 2009.

[29] K. Head, “Propagation of Fatigue Cracks”, Journal of Applied Mechanics, 23:3, pp. 407-410 (1956).

[30] F. McClintock, “The Growth of Fatigue Cracks Under Plastic Torsion”, International Conference on Fatigue of Metals, IME and ASME, p. 538, 1956.

[31] Smith et al, “Comparison of Fatigue Strength, of Bare and Mclad 24S-T3 Aluminum Alloy Sheet Specimens Tested at 12 and 1000 Cycles per Minute” (NACA TN 2231).

[32] S. Begum, D. L. Chen, S. Xub, Alan A. Luo, “ Low cycle fatigue properties of an extruded AZ31 magnesium alloy”, International Journal of Fatigue 31 (2009) pp.726–735.

**Appendix**

**Method of PSA calculation and plot:**

1. Find X (strain column) and Y (stress column) Zero point (starting point) of 1st cycle by plotting stress data and wavelength respectively. In the plot from the pick point to find the highest change point by row number or by time. The formula of calculating the cycle range: highest change row number = (xxxx -250) is the start point of the first cycle and {(xxxx-250) + 1000}-1= xxxx is the end point of the cycle. For subsequent cycles need to increase thousand points.

2. Create a new excel sheet or file copying "strain" and "stress" column using paste value and to add a new column as 'row id'. Add condition column to find out when y value changes from positive to negative, IF ((B2*B3<=0)*(B2<>0),1,0) then result will be 0 or 1. Also add check x at y=0 column, IF (D2=0, 0, (C3*B2-C2*B3)/(B2-B3)) where B is stress column C is strain column and D is condition column.

3. Create a new excel sheet / file copying 'row id' and 'calculate x' using paste value.
   (i) To select data, highlights any point of 'calculate' x column and sort data by smallest to largest value.To delete the rows with zero values.
   (ii) Again, to select data, highlight any point at 'row id' and sort by smallest to largest. This will give $X_1$ and $X_2$ value of shifting range for plastic deformation.
   (iii) Now to calculate PSA = $(X_1-X_2)/2$, fx =$(B_2-B_3)/2$ or $(B_3-B_2)/2$

4. Create a new excel sheet/file copying "row id" and "PSA" column by paste value.
   (i) Select data, highlight any PSA point and sort by smallest to largest.
   (ii) Delete empty rows.
   (iii) Again, sort out by "row id" smallest to largest.
   (iv) Divide PSA column by 100 to get percentage (%) value.
   (v) Insert a new column at the beginning of the table as cycle number.
   (vi) Plot PSA% vs. Cycles [High light these two column-Insert-Scatter-select picture].
   (vi) The plotted curve will be in the positive region. The curve will be either ascending or descending depending on the hardening or softening characteristics of the material.